applied sciences

MDPI

Article

Seismic Strengthening of R/C Buildings Retrofitted by New Window-Type System Using Non-Buckling Slit Dampers Examined via Pseudo-Dynamic Testing and Nonlinear Dynamic Analysis

Kang-Seok Lee [1], Bok-Gi Lee [2] and Ju-Seong Jung [3,*]

[1] Department of Architectural Engineering & Smart City Engineering, Hanyang University, Ansan 15588, Korea; ksleenist@hanyang.ac.kr
[2] Department of Architectural Engineering, Hanyang University, Ansan 15588, Korea; dlqhrrl15@naver.com
[3] Innovative Durable Building and Infrastructure Research Center, Hanyang University, Ansan 15588, Korea
* Correspondence: jjsshm@naver.com; Tel.: +82-31-400-5186

Abstract: In the present study, a window-type seismic control system (WSCS) using non-buckling slit dampers (NBSDs) was proposed and developed to address the disadvantages of conventional seismic control systems so that it can be effectively applied to existing reinforced concrete (RC) buildings. Materials testing was also conducted to examine the material performance and energy dissipation capacity of NBSD. A full-scale two-story test frame modeled from existing RC buildings with non-seismic details was subjected to pseudo-dynamic testing. As a result, the effect of NBSD-WSCS, when applied to existing RC frames, was examined and verified, especially as to its seismic retrofitting performance. In addition, based on material testing and pseudo-dynamic test results, a restoring force characteristics model was proposed to implement the nonlinear dynamic analysis of a test building retrofitted with NBSD-WSCS. Based on the proposed restoring force characteristics, nonlinear dynamic analysis was conducted, and the results were compared with those obtained by the pseudo-dynamic tests. Finally, in an attempt to commercialize this NBSD-based WSCS, nonlinear dynamic analysis was conducted on the entire RC building with non-seismic details retrofitted with NBSD-WSCS. The results showed that the RC frame (building) with no reinforcement applied underwent shear failure at seismic intensity of 200 cm/s^2, a typical threshold applied in seismic design in Korea. In contrast, in the frame (building) retrofitted with NBSD-WSCS, only minor earthquake damage was expected, and even when the seismic intensity was set to 300 cm/s^2, the maximum intensity that had been observed in Korea, only small or moderate seismic damage was expected. These results confirmed the effectiveness of the seismic retrofitting method using NBSD-WSCS developed in the present study.

Keywords: window-type seismic control system; reinforced concrete; non-buckling slit damper; seismic strengthening; seismic capacity; pseudo-dynamic testing; nonlinear dynamic analysis

check for updates

Citation: Lee, K.-S.; Lee, B.-G.; Jung, J.-S. Seismic Strengthening of R/C Buildings Retrofitted by New Window-Type System Using Non-Buckling Slit Dampers Examined via Pseudo-Dynamic Testing and Nonlinear Dynamic Analysis. *Appl. Sci.* **2022**, *12*, 1220. https://doi.org/10.3390/app12031220

Academic Editor: Chiara Bedon

Received: 23 December 2021
Accepted: 19 January 2022
Published: 24 January 2022

1. Introduction

Concrete structures may be highly prone to early degradation and damage, especially in their most vulnerable parts, if they have been improperly designed and constructed or built with inappropriate materials, or when the environmental conditions are severe. This leads to a significant degradation in their safety, durability, and functionality, thereby increasing the frequency and scale of natural disasters and safety accidents. In particular, safety accidents are rapidly increasing in concrete buildings, and the resultant damage is also increasingly severe in scale and scope. The aging and degradation of buildings and their structural performance are accelerated by the degradation of the performance and functionality of their concrete parts, and this degradation process is considered to be caused by a variety of factors, as mentioned above, such as the natural aging of structures; environmental changes, including climate change; quality errors in design and construction; and changes in the load condition due to extension or design change. All these factors pose a serious threat to the overall safety of the buildings. Concrete buildings can be effectively used and fully implement their functionality over the required or intended period of time only when their safety is thoroughly monitored and reviewed at all times. Moreover, when damage occurs or may occur, maintenance and retrofitting measures must be immediately taken to ensure safety.

The world has recently seen large-scale earthquakes caused by environmental changes, including climate change, increasingly causing significant damage to various facilities, and especially buildings and structures. In Japan, China, and Taiwan, the neighboring countries of the Korean Peninsula, earthquake-induced damage is dramatically increasing. In some way, this implies that Korea is not free from the danger of earthquakes, whether directly or indirectly. Notably, the 2005 Fukuoka Earthquake in Japan [1], the 2008 Sichuan Earthquake in China [2], and the 2016 Kumamoto Earthquake in Japan [3] all occurred within the Eurasian Plate to which the Korean Peninsula belongs. This is explicit evidence that large-scale earthquakes may occur in Korea as well.

As is well-known, the 2016 Gyeongju Earthquake and the 2017 Pohang Earthquake in the country [4] already revealed the vulnerability of facilities and buildings in the region in terms of seismic safety to a significant extent. These accidents were a huge wake-up call to the possibility of nationwide disasters. In the 2016 Gyeongju Earthquake, not many buildings or structures were subject to severe damage, except for some column damage in buildings located near the epicenter, including schools and residential buildings. In the 2017 Pohang Earthquake, however, newly built piloti structures and multi-unit dwellings (apartment buildings), including school facilities with non-seismic details, underwent severe damage. In particular, reinforced concrete (RC) columns without sufficient shear reinforcement were found to be highly vulnerable to shear failure, as shown in Figure 1, which then emerged as an urgent and important issue to be addressed in the country's seismic policy development for years to come [4].

Figure 1. RC buildings damaged by shear failure after the 2017 Pohang Earthquake.

In Korea, the seismic design criteria were first established in 1988; six or more-story buildings or those with a gross floor area of at least 100,000 m^2 were subjected to seismic design. Afterward, in 2005, the criteria extended to include three or more-story buildings or those with a gross floor area of at least 1000 m^2 and, in 2015, further to three or more-story buildings or those with a gross floor area of at least 500 m^2 [5]. After the 2016 Gyeongju Earthquake, the criteria were further strengthened to also include two or more-story buildings or those with a gross floor area of at least 500 m^2, which have been in place since February of 2017. As demonstrated in the earthquakes in Gyeongju and Pohang, earthquakes are increasing in Korea in both frequency and intensity. Thus, to prevent buildings from collapsing in case of a large-scale earthquake while minimizing resultant human and property damage, it is necessary to develop an economical and effective seismic retrofitting method to improve the seismic performance of structures that are likely to be vulnerable to earthquakes, and especially RC buildings with non-seismic details, which are highly likely to undergo shear failure in their columns. Moreover, these seismic retrofitting measures must be conducted in an efficient and economical manner based on the expected earthquake magnitude and resultant damage.

Conventional methods for retrofitting the seismic performance of existing RC buildings are mostly based on approaches using stiffening members, such as reinforcing bars, PC, structural steel, and steel plates, or extending cross-sections by placing additional concrete. Additional wall installation, cross-sectional extension, steel-plate reinforcement, steel-brace reinforcement methods are among the most widely used conventional seismic retrofitting methods [6–11]. However, these conventional methods come with the following disadvantages [8].

- Add to the overall weight of buildings. Given the weak foundations of domestic RC buildings with non-seismic details, the application of such methods may require foundation reinforcement work to support the weight increase.
- Difficult to secure enough workspace during the retrofitting process.
- Among the most widely used retrofitting methods, steel-plate reinforcement involves difficulties in material transport and pressing work due to the weight of used steel plates. When steel plates are pressured against affected structures, in particular, it is difficult to determine if the substrate and steel plates have properly adhered to each other. In some cases, such a reinforcement rather negatively affects the building with the reinforced steel plates being suspended from the substrate, instead of supporting it.
- Require construction precision.

In attempts to addressing the disadvantages of conventional repair and retrofitting methods, as mentioned above, research has been actively carried out since the early 1990s on retrofitting methods using new composite materials, such as carbon fiber, Aramid fiber, and glass fiber [12–16]. These methods, however, also come with disadvantages as follows [16]:

- Require pretreatment to treat rough surfaces.
- Involve reinforcement anisotropy, where the degree of reinforcement varies depending on the directions in which fibers are aligned.
- Allow limited workspace, especially for construction work in a narrow space.

As described above, at a time when there is an urgent and increasing need for measures to address earthquake hazards (seismic retrofitting), conventional seismic retrofitting methods, such as additional wall installation, cross-sectional extension, steel-plate reinforcement, steel-brace reinforcement, and other methods using new composite materials, have some disadvantages to be actually applied to domestic buildings and structures, e.g., weight increase and cost-effectiveness.

The recent demand from the public for more active measures to ensure the seismic stability of buildings against earthquakes has led to the development and implementation of various seismic structural control systems. The US's ASCE 7–10 [17] provides specific procedures to implement seismic control design, separately for both seismic control systems, including dampers and earthquake resistance systems. Korea's KDS 41 [5] also provides criteria for the design of seismic control systems, including seismic isolation and damping structures, to be applied in structural design. In general, however, these conventional seismic control systems [18,19] are installed in the construction phase. This then makes it difficult to install such seismic control systems because they need to be added to buildings that have already been built, thereby excessively increasing the overall construction costs. There is also a possibility that these systems, once installed, may fail to achieve the desired seismic retrofitting effects for the given seismic load due to the occurrence of construction errors or buckling. If this is the case, the installed seismic control systems will not be able to effectively support and control the building, proving that they were unnecessary in the first place. Furthermore, these systems are not highly suitable for the external design of buildings, which require aesthetic features. These systems are also difficult to apply to the seismic retrofitting RC buildings, which are relatively less deformable than steel frame buildings. Thus, to overcome the disadvantages of existing seismic control systems, as described above, it is necessary to develop a system based on a completely new concept.

According to necessity of a new retrofit method, new retrofit approaches have also been applied to existing RC buildings. These can reduce structural damage to existing RC buildings by concentrating seismic energy dissipation on reusable damping devices [20,21]. More recently, studies have been carried out on hybrid damping devices with combined behavior. Ibrahim et al. proposed a visco-plastic damper which combines a displacement-dependent device and velocity-dependent device [22]. Chang-Hwan Lee et al. devised a hybrid passive control device comprising a friction damper and a metalic damper [23], and F. Sutcu et al. proposed buckling-restrained brace and steel frames system [24], O. Ramazan et al. and M. Ferraioli et al. verified the seismic performance of buckling-restrained brace [25,26]. M.N. Eldin et al. proposed self-centering PC reinforcement frames [27]. C. Bedon et al. proposed a vibration control technology using a passive system for curation walls and verified it analytically [28–30]. In addition, research on various reinforcement design methods to which the energy dissipation device is applied is being conducted using single-degree-of-freedom models [31–33].

In the present study, a window-type seismic control system (WSCS) using non-buckling slit dampers (NBSDs) was proposed and developed to address the disadvantages of conventional seismic control systems so that it can be effectively applied to existing RC buildings through review of previous research paper. Materials testing was also conducted to examine the material performance and energy dissipation capacity of the steel NBSD system. A full-scale two-story test frame modeled from existing domestic RC buildings with non-seismic details was subjected to pseudo-dynamic testing. As a result, the effect of NBSD-WSCS, when applied to existing RC frame structures, was examined and verified, especially as to its seismic retrofitting performance. In addition, based on material testing and pseudo-dynamic test results, a restoring force characteristics model was proposed to implement the nonlinear dynamic analysis of a test building retrofitted with NBSD-WSCS. Further, based on the proposed restoring force characteristics, nonlinear dynamic analysis was conducted, and the results were compared with those obtained by the pseudo-dynamic tests.

Finally, in an attempt to commercialize this NBSD-based WSCS, nonlinear dynamic analysis was conducted on the entire RC building with non-seismic details retrofitted with NBSD-WSCS. The seismic response load-displacement characteristics, energy dissipation capacity, and degree of seismic damage based on the ductility of used members before and after the reinforcement were examined and compared to determine the corresponding seismic retrofitting performance.

2. Overview of the Seismic Retrofitting Method Using the NBSD-Based WSCS

Among various seismic control dampers, steel silt dampers are most widely used as seismic structural control systems because they are easy to design and build, cost-effective, structurally stable, and capable of effectively absorbing earthquake input energy. However, Kafi and Hoosh [34] reported that steel silt dampers were highly likely to involve out-of-plane seismic forces and buckling along the axial direction, thereby leading to a decrease in their seismic energy dissipation capacity. In the present study, a novel window-type seismic control system (WSCS) using non-buckling slit dampers (NBSDs) was proposed, as shown in Figure 2. This system is equipped with hinges and buckling prevention plates to prevent the occurrence of buckling, which directly causes its energy dissipation capacity to decrease, so that the applied seismic energy can be effectively dissipated. As such, this system can be suitably applied to existing RC buildings for seismic reinforcement.

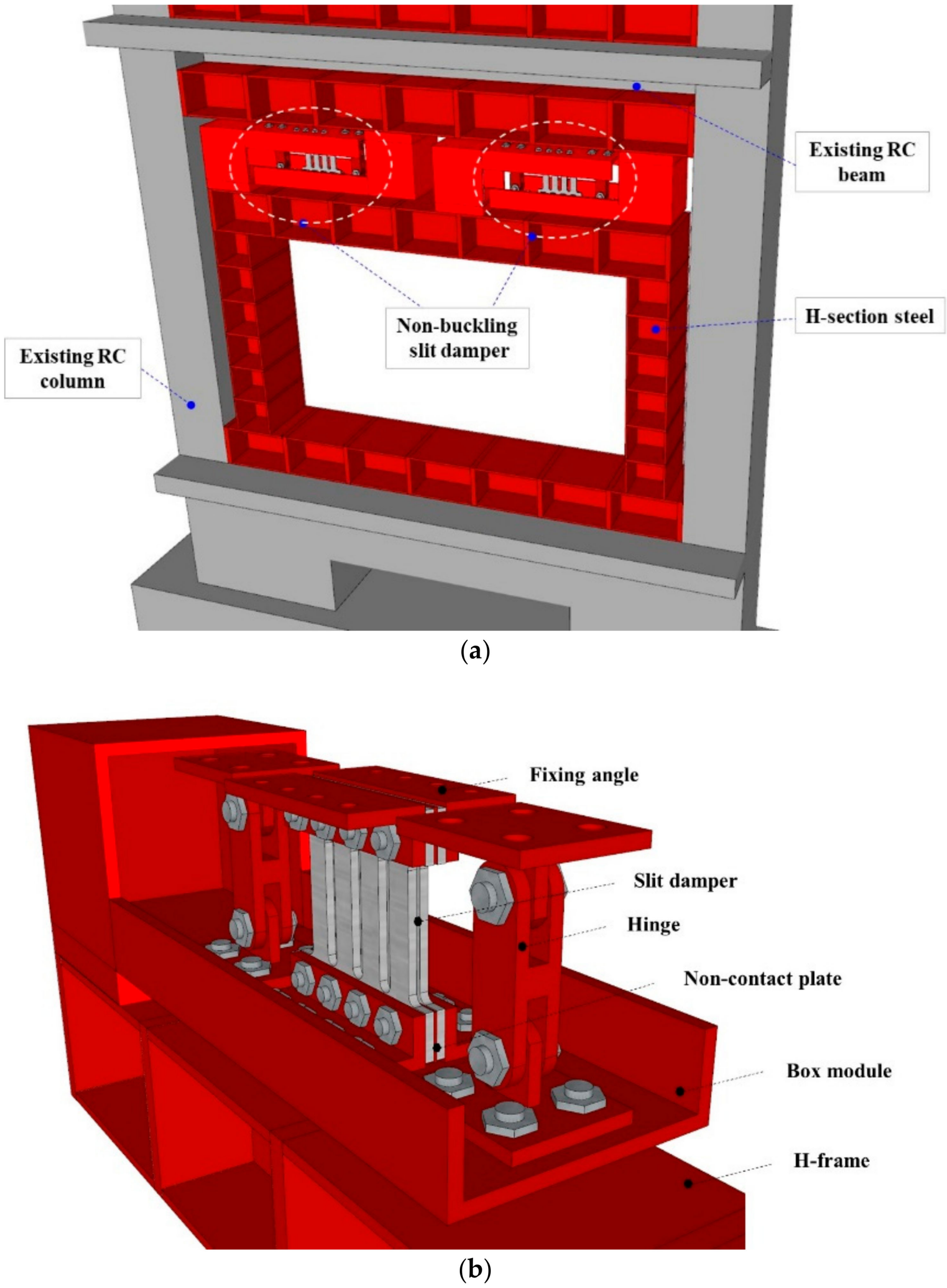

Figure 2. A schematic diagram of the window-type seismic control system using non-buckling slit dampers (NBSDs): (**a**) the window-type seismic control system, (**b**) components of the NBSD.

As shown in Figure 2, the NBSD-based WSCS is composed of an H-frame into which steel slit dampers are assembled, along with box modules and hinges to prevent the buckling of these dampers, i.e., preventing the out-of-plane buckling of the struts while only allowing for in-plane lateral deformation to effectively absorb seismic energy.

3. Material Testing of Window-Type NBSDs and the Results

3.1. Material Test Plans for NBSDs and Their Mechanical Properties

In an attempt to verify the seismic performance of the NBSD-WSCS developed in the present study, full-scale specimens were prepared and then subjected to material testing in which the lateral load corresponding to the displacements required to achieve the target performance was applied to the specimens in a repetitive manner. Figure 3 presents the detailed specifications of the NBSDs used in the material testing. The used NBSDs were made of SS275. Three Type 5 tensile specimens were taken from the steel plates used to fabricate the dampers according to KS B0801 (Tensile test specimens for metals) [35] and then subjected to tensile tests according to KS B 0802 [36]. The results showed that the average yield and tensile strengths were 282 and 418 MPa while the average elongation was 24.4%. The yield proof stress and yield displacement of the NBSD were estimated using Equations (1)–(4) below [37,38].

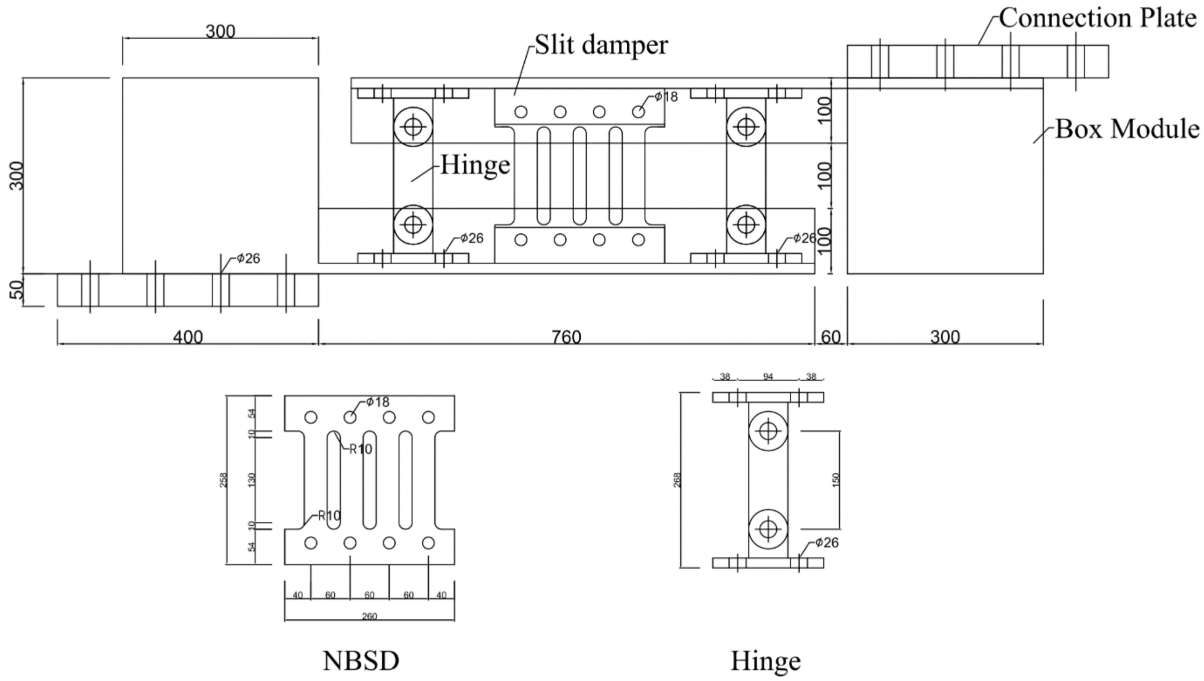

Figure 3. Detailed descriptions of the NBSDs used in the material testing.

$$Q_{yb} = n \cdot \frac{tB^2F_y}{2H} \tag{1}$$

$$Q_{ys} = n \cdot \frac{2tBF_y}{3\sqrt{3}} \tag{2}$$

$$Q_{du} = \min\left[Q_{yb} \cdot Q_{ys}\right] \tag{3}$$

$$\delta_{du} = \frac{1.5Q_{dy}(H+2r)}{nEtB}[\left(\frac{H'}{B}\right)^2 + 2.6] \tag{4}$$

Here, Q_{yb}: damper bending yield proof stress, Q_{ys}: damper shearing yield proof stress, Q_{du}: damper yield proof stress, δ_{du}: damper yield displacement, n: Number of struts, F_y: yield strength of the steel plate, t: damper thickness, r: fillet radius, B: Strut width, E: elastic modulus, H: Strut height, H' : $H + \frac{2r^2}{H+2r}$.

Table 1 presents a list of NBSD specimens and the corresponding calculation results. Two identical NBSD specimens were prepared and tested, and the design yield strength and yield displacement were estimated to be 102.6 kN and 0.69 mm, respectively.

Table 1. NBSD specimens used in the material testing and the corresponding calculation results.

Specimen Name	Number of Dampers Used (N)	Yield Strength of the Steel Plate (MPa)	Thickness (mm)	Fillet Radius (mm)	Strut Width (mm)	Strut Height (mm)	Number of Struts (n)	Design Yield Strength (Kn)	Design Yield Displacement (mm)
NBSD-1	2	275	10	10	35	130	4	102.6	0.69
NBSD-2									

3.2. NBSD Material Test Loading and Measurement Methods

Hysteretic steel dampers serve to dissipate energy through their plastic behavior following yielding, and their energy dissipation capacity is proportional to the displacement applied, i.e., displacement dependent. Thus, both maximum and repetitive deformation capacities are dominant factors that determine the overall performance of hysteretic steel dampers. In the present study, material testing was conducted according to KDS 17 10 00 (Seismic Building Design Code) [5]. Detailed descriptions of the applied NBSD specimen and measuring device setup are presented in Figure 4.

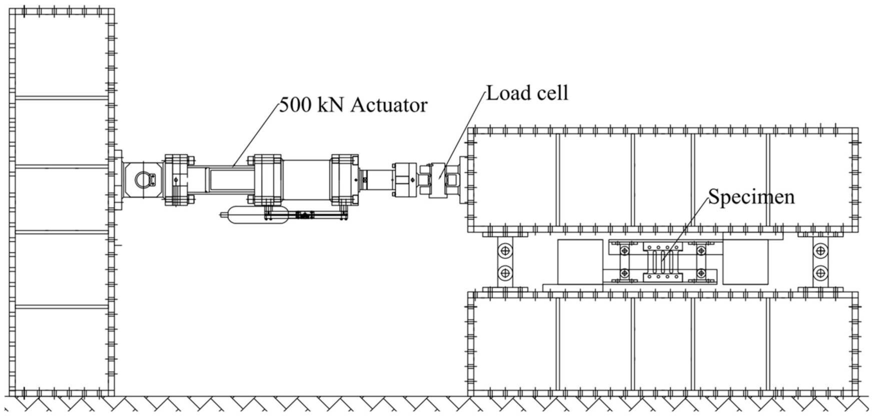

(**a**)

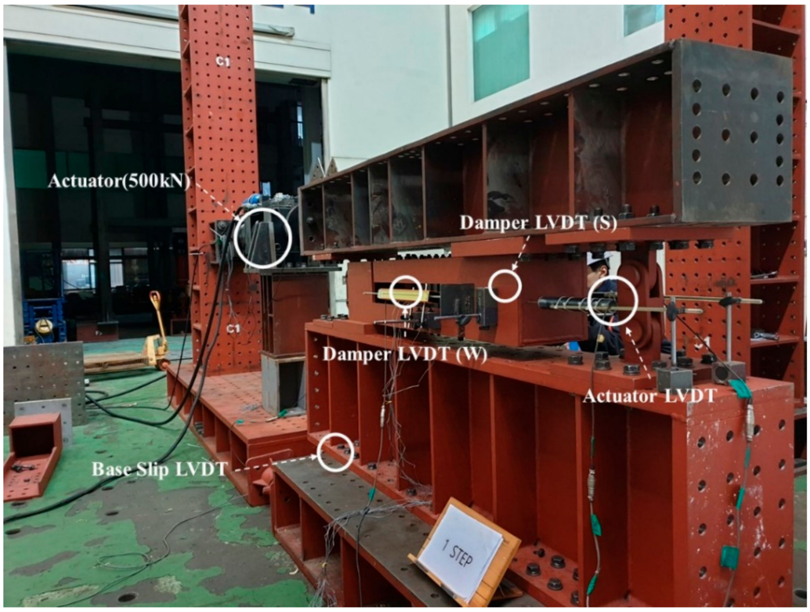

(**b**)

Figure 4. Specimen and measuring device setup: (**a**) schematic test setup and (**b**) actual setup image.

The lateral force was applied to the specimens using an actuator, and the actuator's loading points were aligned with the center of the upper steel structure for loading on top of the specimens. According to "17.6 Device Prototype Test of KDS 41 17 10 00 (Seismic Building Design Code) [5]," the specimens were subjected to static cyclic loading with the respective displacements 0.33 times the expected device displacement for ten times, 0.67 times the expected device displacement for five times, and 1.0 times the expected device displacement for three times (See Figure 5). The maximum device displacement when the maximum-magnitude earthquake was considered was set to 1% (33 mm), which corresponded to the allowable inter-story displacement angle of school buildings (special grade) as the target subjects [37].

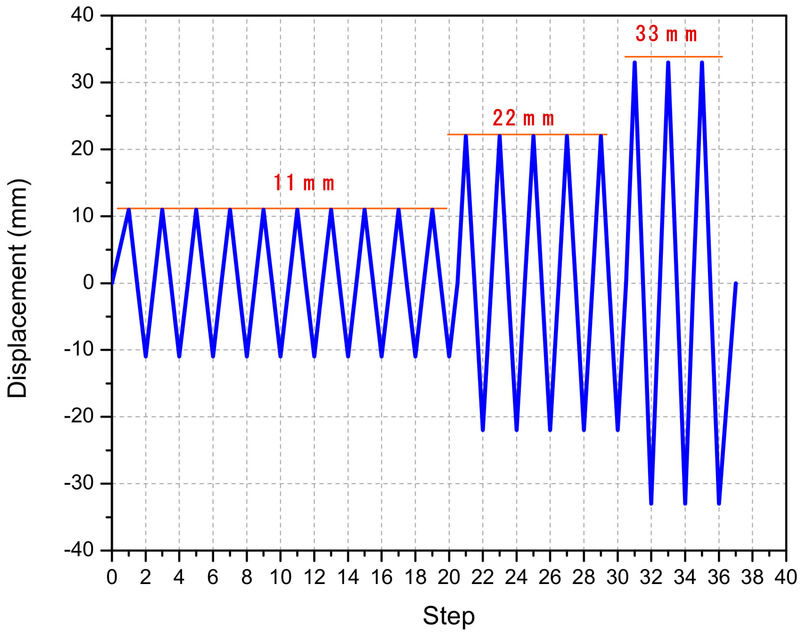

Figure 5. Cyclic loading plan.

3.3. NBSD Material Test Results and Analysis

(1) Load-displacement curves

Load-displacement curves were obtained from NBSD-1 and NBSD-2, as shown in Figure 6, and images of the specimens after the maximum control displacement of 33 mm was reached are presented in Figure 7. These results are summarized in Table 2. The yield proof stress (Q_{dy}) and yield displacement (δ_{dy}) results provided in Table 2 were determined as follows. First, a line with a slope one-third that of the corresponding initial stiffness line was drawn, and a tangent line between this line and the corresponding load-displacement curve was determined. The intersection between the obtained tangent line and the initial stiffness line was then defined as referring to the yield displacement (δ_{dy}) and yield proof stress (Q_{dy}) [38,39].

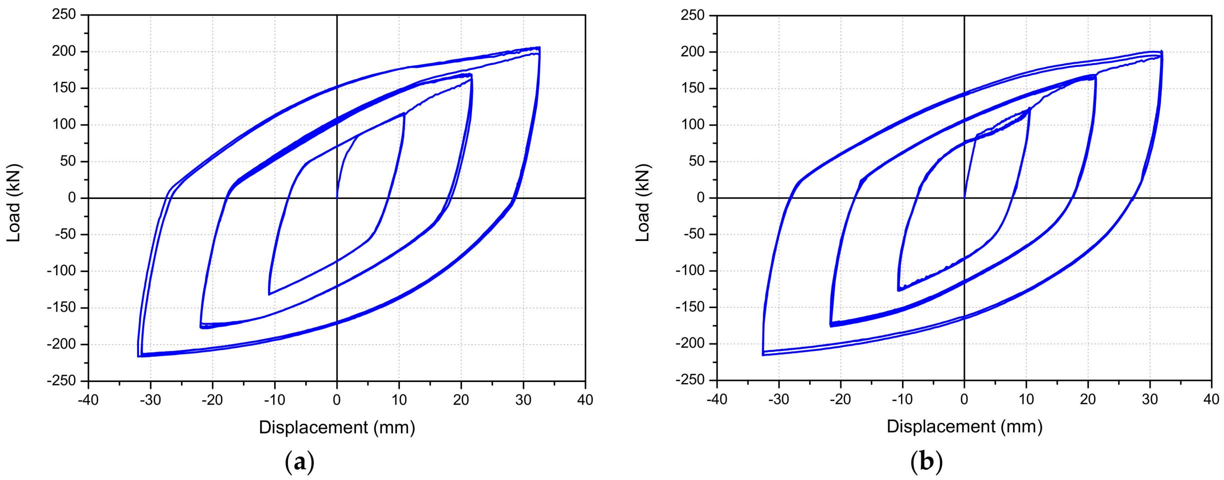

Figure 6. Load-displacement curves: (**a**) NBSD-1 and (**b**) NBSD-2 specimens.

Figure 7. Images of the specimens at the maximum control displacement of 33 mm.

Table 2. Test results obtained from the NBSD specimens.

Specimen Name	Maximum Control Displacement ($\delta_{d,max}$)	Yield		Positive Load		Negative Load		k_{dy} (kN/mm^2)
		δ_{dy} (mm)	Q_{dy} (kN)	δ_d (mm)	Q_d (kN)	δ_d (mm)	Q_d (kN)	
NBSD-1	33	1.49	76.0	32.6	205.9	32.5	216.5	51.0
NBSD-2		1.56	80.8	32.3	201.6	32.6	215.5	51.7

δ_{dy}: damper yield displacement, Q_{dy}: damper yield proof stress, δ_d: maximum damper displacement, Q_d: maximum damper yield proof stress, k_{dy}: damper yield stiffness.

For NBSD-1, the yield displacement δ_{dy} was 1.49 mm, the yield proof stress Q_{dy} was 76.0 kN, and the maximum proof stress was Q_d =216.3 kN. For NBSD-2, the yield displacement δ_{dy} was 1.56 mm, the yield proof stress was Q_{dy} =80.8 kN, and the maximum proof stress Q_d was 215.5 kN. As such, the two specimens showed very similar results.

(2) Equivalent damping ratios and energy dissipation

The performance of seismic control systems can be determined by their ability to dissipate the seismic energy input, which is characterized by effective stiffness, energy dissipation capacity, and equivalent damping ratios. As shown in Figure 8b, the elastic potential energy (E_{So}) of a seismic control system can be calculated based on its effective stiffness ($k_{d,eff}$) illustrated in Figure 8a. Its cumulative energy dissipation (E_D) can also be calculated based on the concept described in Figure 8b. The equivalent damping ratio (β_{eq}) can be determined using the elastic potential energy (E_{So}) in Equation (5) and the cumulative energy dissipation (E_D) [17,40].

$$\beta_{eq} = \frac{1}{2\pi} \cdot \frac{E_D}{k_{d,eff}(i) \cdot \delta_{ave}^2} = \frac{1}{4\pi} \cdot \frac{E_D}{E_{So}} \quad (5)$$

Here, $E_D(i)$: total cumulative energy dissipation (i: 11, 22, 33 mm), $k_{d,eff}(i)$: effective stiffness of the seismic control system (i: 11, 22, 33 mm), and δ_{ave}: average absolute value of displacements ($|\delta_{d,min} + \delta_{d,max}|/2$).

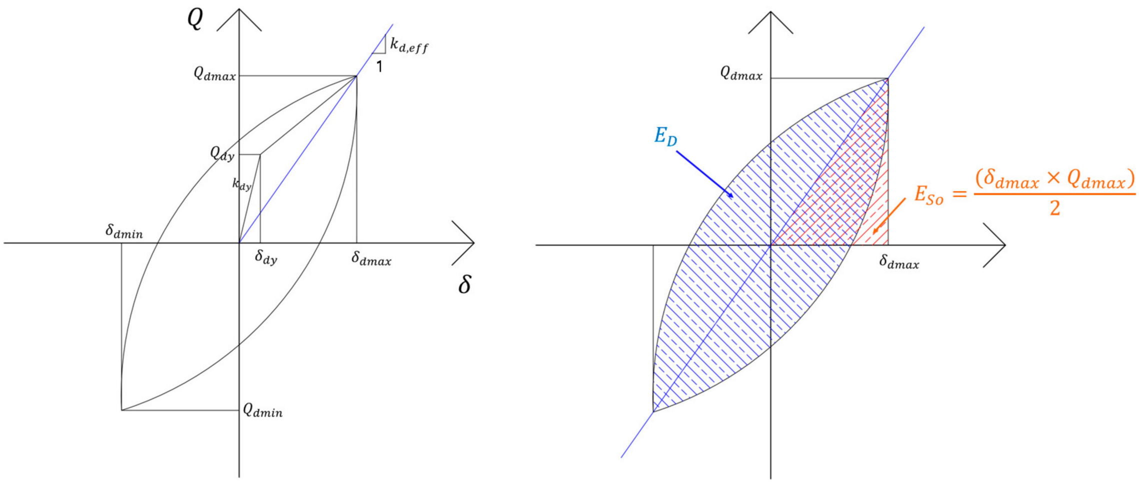

(a) (b)

Figure 8. Concepts of effective stiffness, elastic potential energy, and energy dissipation in seismic control systems: (**a**) effective stiffness and (**b**) elastic potential energy and cumulative energy dissipation.

The effective stiffnesses ($k_{d,eff}$) of the NBSD specimens are provided in Table 3, and the equivalent damping ratios (β_{eq}) and cumulative energy dissipation (E_D) were estimated based on the measured effective stiffnesses, as shown in Table 4. The average effective stiffnesses ($k_{d,eff}$) of the NBSD specimens were 11.6 kN/mm (11 mm), 7.3 kN/mm (22 mm), and 6.4 kN/mm (33 mm), respectively. The average cumulative energy dissipation ($E_{D,ave}$) was measured to be 117.8 kN·m. The average equivalent damping ratios ($\beta_{eq,ave}$) were 0.31 (11 mm), 0.38 (22 mm), and 0.38 (33 mm), respectively. The results showed that the equivalent damping ratios increased with increasing displacements, indicating that energy can be efficiently dissipated even when the deformation is large. Accordingly, this NBSD system was expected to provide an excellent damping effect when applied to RC buildings.

Table 3. Effective stiffnesses of the NBSD-based seismic control system.

Specimen Name	Stiffness (kN/mm)			
	k_{dy}	$k_{d,eff}(11)$	$k_{d,eff}(22)$	$k_{d,eff}(33)$
NBSD-1	51.0	11.4	6.6	6.5
NBSD-2	51.7	11.8	8.1	6.4

k_{dy}: damper yield stiffness and $k_{d,eff}(i)$: effective stiffness of the seismic control system (i = control displacement: 11, 22, 33 mm).

Table 4. Equivalent damping ratios and cumulative energy dissipation of the NBSD-based seismic control system.

Specimen Name	Control Displacement (mm)	$E_{D,ave}(i)$ (kN·m)	$E_{So}(i)$ (kN·m)	β_{eq}	$\beta_{eq,ave}$	$E_{D,total}(i)$ (kN·m)
NBSD-1	11	2.79	0.69	0.32	0.36	119.5
	22	8.43	1.6	0.42		
	33	17.01	3.54	0.38		
NBSD-2	11	2.67	0.71	0.3	0.34	116.1
	22	8.19	1.96	0.34		
	33	16.54	3.48	0.38		

$E_{D,ave}(i)$: average energy dissipation for one cycle of control displacement, $E_{So}(i)$: elastic potential energy, β_{eq}: equivalent damping ratio, $\beta_{eq,ave}$: Average equivalent damping ratio, and $E_{D,total}(i)$: total cumulative energy dissipation (i: 11, 22, 33 mm).

(3) Performance criteria for the NBSD-based seismic control system

As mentioned above, cyclic loading tests were conducted according to the test methods using displacement-controlled seismic control systems provided in "17.6 Tests of Dampers of KDS 41 17 00: 2019 [5]." Based on the test results, the performance of the seismic control system was evaluated against the criteria shown in Table 5 [5]. Both NBSD-1 and NBSD-2 developed in the present study were tested for performance conformance, and the results are presented in Tables 6 and 7, respectively. All conformance tests were conducted while the maximum displacement of 33 mm was applied. The results showed that the NBSD specimens met the performance requirements for displacement-controlled seismic control systems.

Table 5. Performance criteria for displacement-controlled seismic control systems.

Criterion	Performance Requirements
1	During cyclic loading for a certain number of cycles, both maximum load (Q_{max}) and minimum load (Q_{min}) measured at the zero-displacement point are required to be within 15% of the average of all measured loads.
2	During cyclic loading for a certain number of cycles, the loads measured in each direction at the maximum device displacement are required to be within 15% of the average of all measured loads.
3	During cyclic loading for a certain number of cycles, the area of hysteresis loop measured from the damper (E_D) is required to be within 15% of the average of all measured hysteresis loop areas ($E_{D,ave}$).

Table 6. Conformance evaluation of NBSD-1 as a seismic control system.

Division	Performance Requirements				
Criterion 1	Cycle	1	2	3	Average
	Q_{max} (kN)	153.4	153.1	154.1	153.3
	Q_{min} (kN)	−167.9	−169.8	−171.7	−169.8
	$(Q_{max} - Q_{ave})/Q_{ave}$	−0.0001	−0.002	0.003	
	$(Q_{min} - Q_{ave})/Q_{ave}$	−0.01	0	0.01	
	Results	Conforming	Conforming	Conforming	-
Criterion 2	Cycle	1	2	3	Average
	Q_{max} (kN)	206.1	204.2	196.6	202.3
	Q_{min} (kN)	−212.5	−212.7	−216.4	−213.8
	$(Q_{max} - Q_{ave})/Q_{ave}$	0.01	0.009	−0.02	
	$(Q_{min} - Q_{ave})/Q_{ave}$	−0.006	−0.005	0.01	
	Results	Conforming	Conforming	Conforming	-
Criterion 3	Cycle	1	2	3	Average
	E_D (kN·m)	17.0	16.4	17.7	17.01
	$(E_{\mathrm{D}} - E_{D,ave})/E_{D,ave}$	−0.001	−0.03	0.04	
	Results	Conforming	Conforming	Conforming	-

Table 7. Conformance evaluation of NBSD−2 as a seismic control system.

Division	**Performance Requirements**				
Criterion 1	Cycle	1	2	3	Average
	Q_{max} (kN)	139.7	141.6	144.5	141.9
	Q_{min} (kN)	−160.7	−162.6	−165.9	−163.0
	$(Q_{max} - Q_{ave})\ Q_{ave}$	−0.01	−0.002	0.01	
	$(Q_{min} - Q_{ave})/Q_{ave}$	−0.01	−0.002	0.01	
	Results	Conforming	Conforming	Conforming	-
Criterion 2	Cycle	1	2	3	Average
	Q_{max} (kN)	192.5	196.3	202.0	196.9
	Q_{min} (kN)	−208.7	−212.5	−214.4	−211.8
	$(Q_{max} - Q_{ave})/Q_{ave}$	−0.02	−0.003	0.02	
	$(Q_{min} - Q_{ave})/Q_{ave}$	−0.01	0.002	0.01	
	Results	Conforming	Conforming	Conforming	-
Criterion 3	Cycle	1	2	3	Average
	E_D (kN·m)	16.4	16.1	17.1	16.5
	$(E_{\mathrm{D}} - E_{D,ave})/E_{D,ave}$	−0.008	−0.02	0.03	
	Results	Conforming	Conforming	Conforming	-

4. Overview of Pseudo-Dynamic Testing and Result Analysis

As shown in Figure 9, a full-size two-story test frame modeled from existing RC school buildings with non-seismic details was subjected to pseudo-dynamic testing using the pseudo-dynamic testing system developed in the present study. As a result, the effect of the developed NBSD-WSCS, when applied to existing RC buildings, was examined and verified, especially as to its seismic retrofitting performance, i.e., restoring force characteristics, energy dissipation capacity, and seismic response control.

4.1. Overview of Existing Seismic Test Methods

The impact of an earthquake on a structure depends on the ground acceleration and the type, weight, and stiffness of the structure. The horizontal earthquake acceleration induces shear stress on the vertical members of the structure, which support the structure. This then subjects the structure to relative lateral motion. In general, when an earthquake occurs, many structures, even after large deformation, support themselves without structural collapse. In the process, however, they are likely to absorb some energy through nonelastic behavior. More specifically, while the seismic load is being transmitted to a structure, some materials in the structural system reach their yield points, thereby causing localized plastic deformation to occur. The resultant large amount of earthquake input energy then starts to be absorbed by the structure through nonelastic behavior. It is, however, still very difficult or impossible to theoretically assess such nonelastic behavioral characteristics even though a wide range of relevant computing programs have been developed.

For that reason, the nonelastic seismic response of a structure has been mostly experimentally studied with various test methods, including shaking table tests, quasi-static tests, and pseudo-dynamic tests. The shaking table test method is considered to be the most effective way to assess the seismic behavior of structures, but the maximum weight and size of specimens are limited by the size and capacity of the applied shaking table. Thus, in most cases, reduced-size models are used, and this may lead to issues arising from the discrepancy between the model and the actual structure. In an attempt to overcome this limitation, quasi-static tests have been widely used to assess the nonelastic behavior of full-size structures, in which the test conditions are controlled by the displacement or load.

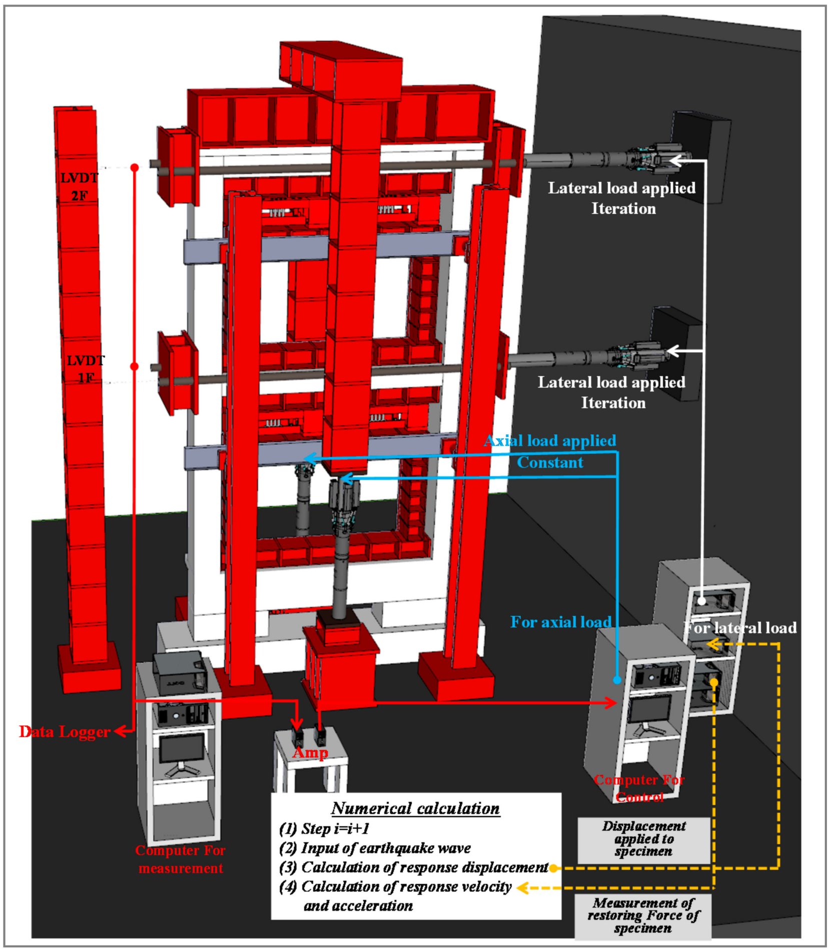

Figure 9. Illustration of the pseudo-dynamic testing system developed in the present study.

Meanwhile, pseudo-dynamic testing was designed and developed to have only the advantages of both the shaking table test and the quasi-static test methods [41]. It is a hybrid experimental and numerical approach that combines experimental techniques with numerical analysis. Pseudo-dynamic testing is composed of two parts: numerical analysis and loading tests on specimens. In the numerical analysis stage, based on the amount of response to a specific deformation, input seismic acceleration, and the amount of response in the current step measured from specimens during the loading test, the corresponding motion equation is calculated using numerical integration, and the response deformation in the next step is estimated. In the loading test stage, the estimated response deformation is then applied to specimens using loading devices, such as an actuator. In the process, the corresponding displacement hysteresis is measured. The procedures described above are conducted in a repetitive manner. In short, response deformation caused by earthquake-like loading is applied to specimens, and then their seismic response is calculated through numerical analysis to determine the seismic response of the target structure.

Pseudo-dynamic testing is very similar to existing quasi-static testing, except that the displacement that is applied to the structure is numerically determined during the test. While most seismic response prediction based on numerical dynamic analysis requires that an assumption about hysteretic characteristics be made, pseudo-dynamic testing allows such information to be directly measured from specimens so that it can implement a seismic response that is very similar to the actual one.

4.2. Pseudo-Dynamic Testing System and Test Methods

Figure 9 is a conceptual illustration of the pseudo-dynamic test system developed in the present study; the figure also shows how specimens are set and tested. As shown in Figure 9, it is a two-degree-of-freedom (TDF) system and composed of the numerical analysis unit, in which the input seismic ground motion is determined by the control computer and the loading test unit in which specimens are actually subjected to testing. The displacement response that has been calculated during the test is actually applied to the specimen using two hydraulic actuators that are installed in the horizontal direction. The restoring force is experimentally measured during the test, and this measurement is fed to the control computer to calculate the corresponding displacement response. Data conversion is performed by an analog-to-digital/digital-to-analog converter (DA-16A) [42], and the seismic response during pseudo-dynamic testing is calculated by the closed-loop control system.

Control computer-based numerical analysis was conducted using the Pseudo-dynamic Testing Program [43]. Based on the restoring force of the specimen against the applied deformation measured with LVDT during the loading test, along with the input seismic acceleration and the measured response in the current step, the amount of response in the next step is calculated through numerical integration using the motion equation, as shown in Equation (6).

$$M\ddot{y}(t) + C\dot{y}(t) + r(t)[= Ky(t)] = -M\ddot{y_0} \tag{6}$$

Here, M, C, and K refer to the mass, damping, and stiffness matrix of the structure, respectively. y refers to the relevant displacement vector of each layer weight for the foundation. r is the restoring force vector, while $\ddot{y_0}$ is the input ground acceleration.

The numerical integration of the motion equation was conducted using the α-method [44], and the numerical integration algorithm for pseudo-dynamic testing is shown in Equations (7)–(9).

$$Ma_{i+1} + (1+\alpha)Cv_{i+1} - \alpha Cv_i + (1+\alpha) - \alpha r_i = (1+\alpha)f_{i+1} - \alpha f_i \tag{7}$$

$$y_{i+1} = y_i + \Delta t v_i + \Delta t^2\left[\left(\frac{1}{2} - \beta\right)a_i + \beta a_{i+1}\right] \tag{8}$$

$$v_{i+1} = v_i + \Delta t[(1-\gamma)a_i + \gamma a_{i+1}] \tag{9}$$

Here, y_i, v_i, and a_i refer to the joint displacement at the time corresponding to $i\Delta t$, velocity, and acceleration, respectively. Δt is the time interval for integration, r_i is the restoring force vector at the joint displacement, and f_i is the external load vector ($-M\ddot{y_0}$).

In an elastic structure, $r_i = Ky_i$ applies (K is the elastic stiffness matrix of the structure). α, β, and γ are parameters that control the numerical characteristics of the algorithm. The conditions $-5 \leq \alpha \leq 0$, $\beta = \frac{(1-\alpha)^2}{4}$, and $\gamma = \frac{1}{2} - \alpha$ indicate that the system is in a state of unconditional stability.

In the next step, the displacement response is calculated based on the stiffness (K), the mass (M), and the coefficient of damping proportional to stiffness (C) using Equations (6)–(9). The damping factor (ξ) was set to 0.03, which amounts to 3% of the critical damping. As shown in Figure 9, the horizontal seismic response deformation is applied on the specimen using two 2000-kN hydraulic MTS actuators on the first and second floors. The horizontal displacement used to calculate the displacement response is measured using a 300-mm linear variable differential transformer (LVDT) installed on each floor. The axial force was constantly applied to each column of the specimen using 1000-kN oil jacks installed on each side of the specimen by properly distributing the axial load applied to the actual existing frame. The Hachinohe wave (EW), which exhibited the largest seismic response displacement (best ductility) among historical seismic waves, was selected [45] and used to determine the seismic ground motion. The acceleration values were set to 200, 300, and 400 cm/s^2, and tests were then conducted using the pseudo-dynamic testing system accordingly.

4.3. Used Materials and Their Properties

The compressive strength of the test frame concrete used in pseudo-dynamic testing was set to 21 MPa. The standard correction factor was determined by averaging the compressive strength of three specimens; 97% of measured compressive strength. As a result, the average 28-day compressive strength was measured to be 21.4 MPa. SD400 (Class 1) was used as reinforcing bars. D19 and D16 were used as longitudinal reinforcing bars for column members, while D10 was used as shear reinforcing bars. Three tensile specimens of reinforcing bars were prepared in accordance with KS B 0801 [35] to examine the material properties of the reinforcing bars used for connection performance test specimens. These specimens were then subjected to tensile testing at a tensile rate of 5 mm/min using a universal tester (U.T.M.). The results showed that the average yield and tensile strength of the reinforcing bars were 491 and 731 MPa for both D19 and D16, respectively, and 477 and 711 MPa for D10, respectively.

4.4. Specimen Preparation and Parameters

A domestic three-story RC school building frame (standard drawings of the 1980s) [46], as shown in Figure 10, was selected and used to verify the seismic performance of the proposed NBSD-based seismic retrofitting method. The story height is 3.3 m, the design concrete strength is 21 MPa. T-shape beams were used as each floor's beams, considering the effective slab width in accordance with KDS 41 [5].

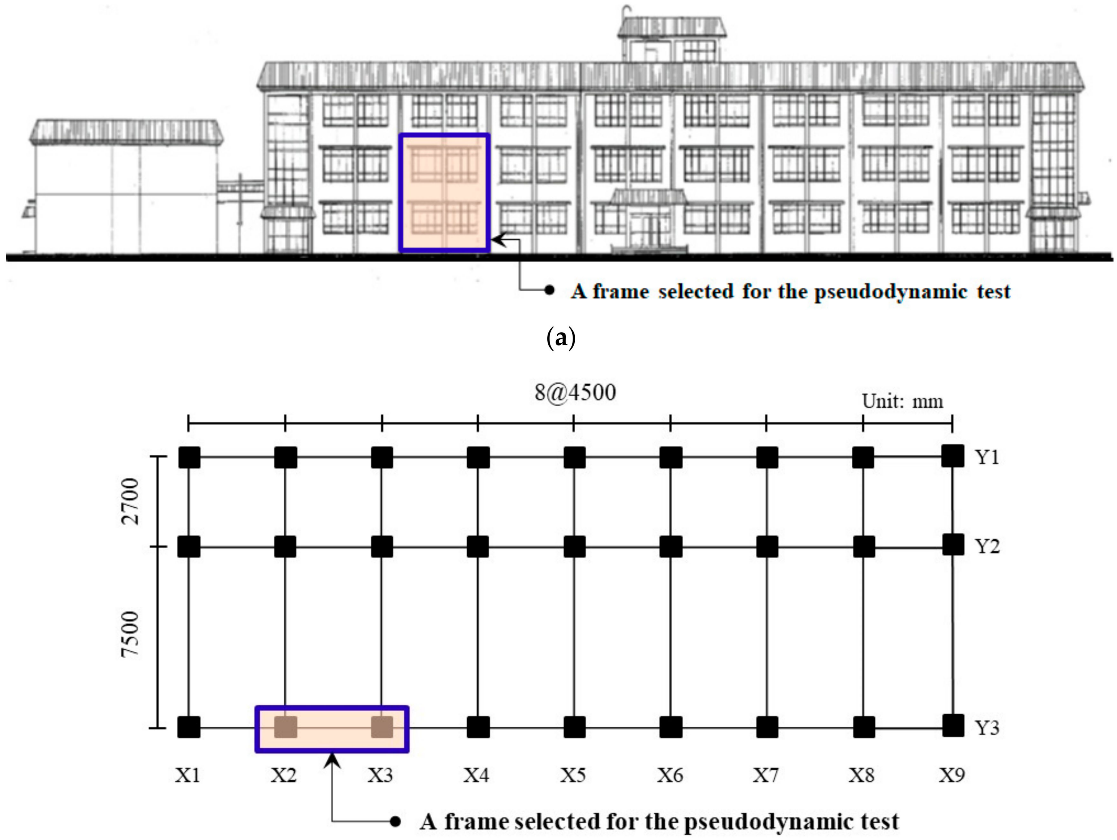

(b)

Figure 10. *Cont.*

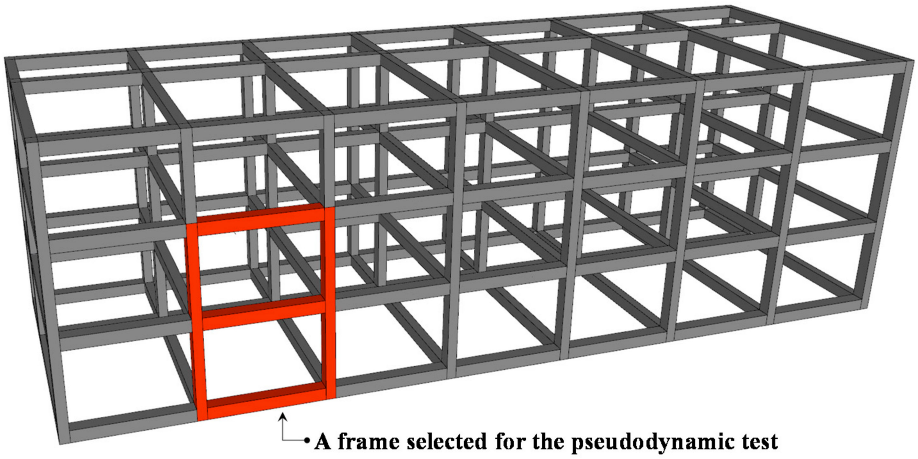

(c)

Figure 10. Images of target building and frames selected for pseudo-dynamic testing: (**a**) front view, (**b**) top view, and (**c**) 3D view.

Figures 11a and 12a show the bar arrangement details of the existing frame with no reinforcement applied, along with an image of the corresponding specimen. For pseudo-dynamic testing, a test WSCS frame retrofitted using the proposed NBSD-based seismic retrofitting method was prepared, along with a test frame with no reinforcement applied for comparison, as shown in Figures 11a and 12a. These two test frames were subjected to the tests, and the results were compared.

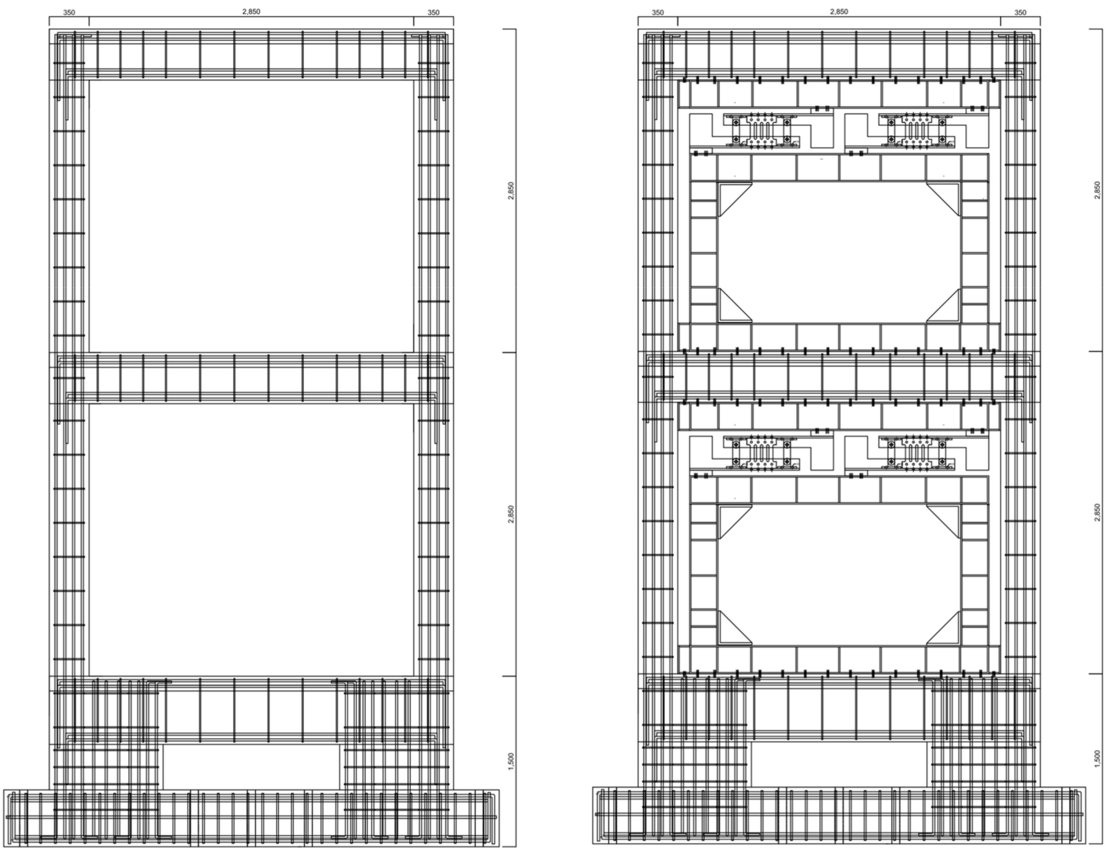

(**a**) (**b**)

Figure 11. Bar arrangement details of the specimens: (**a**) existing frame with no reinforcement applied (PD-FR) and (**b**) frame retrofitted with NBSD-WSCS (PD-NBSD-WSCS).

(a)

(b)

Figure 12. Images of the test specimens: (**a**) existing frame with no reinforcement applied (PD-FR) and (**b**) frame retrofitted with the NBSD-WSCS (PD-NBSD-WSCS).

According to Lee [45], the Hachinohe wave (EW) exhibited the largest seismic response displacement (ductility) among the ten historical seismic waves set for middle- and low-rise RC structures (whose proof stress is less than 0.5 in terms of shear coefficient). Thus, in the present study, the Hachinohe wave was selected as the input seismic ground motion for pseudo-dynamic testing. The input seismic acceleration was set by standardizing the Hachinohe wave (EW) into 200, 300, and 400 cm/s^2. Among them, 200 and 300 cm/s^2 are equivalent to two-thirds the seismic magnitude of an earthquake with a recurrence period of 2400 years (corresponding to Seismic Zone-1 and Soil Profile Type S_4 and S_5) defined in KDS 41 [5]. Furthermore, 400 cm/s^2 was defined to examine the performance of the NBSD-based seismic retrofitting method proposed in the present study when a large-scale earthquake occurs. Thus, it corresponds to the seismic magnitude of an earthquake with a recurrence period of 2400 years. Figure 13 shows time history records of the normalized ground motion accelerations used in the pseudo-dynamic test, respectively, together with their acceleration response spectrum. The axial force was determined based on the axial load exerted on the actual existing frame (two columns), i.e., 1000-kN. Thus, each of the two columns was subjected to a constant axial force of 500-kN. Table 8 summarizes the applied specimen parameters.

Table 8. Pseudo-dynamic testing specimens and the applied parameters.

Specimen Name	Test Method	Reinforcing Method	Input Seismic Wave Intensity (cm/s^2)
PD-FR	Pseudo-dynamic testing	-	200
PD-NBSD-WSCS	Pseudo-dynamic testing	The NBSD-based window-type seismic control system	200/300/400

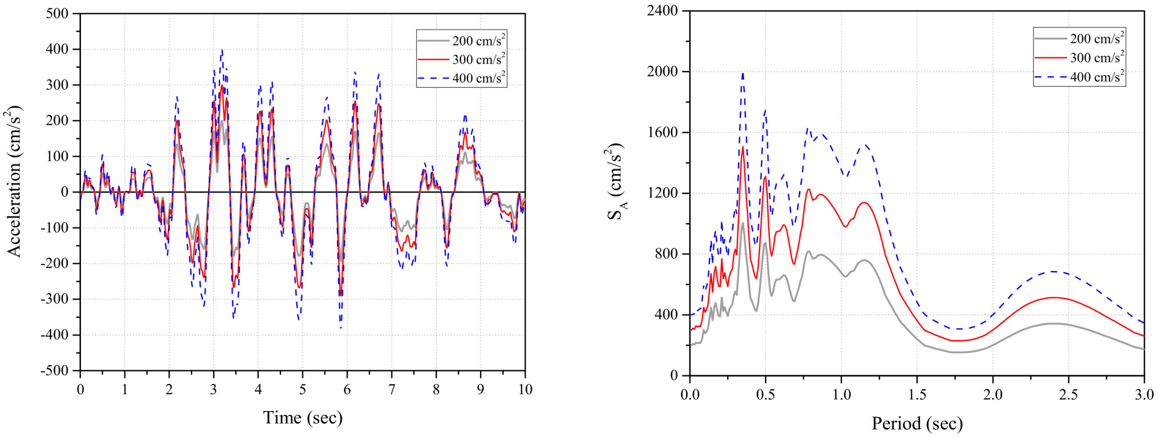

(**a**) (**b**)

Figure 13. Ground motion accelerations used in the pseudo-dynamic test: (**a**) time history records and (**b**) acceleration response spectrum.

4.5. Experimental Results and Analysis

Both the test specimen with no reinforcement applied (PD-FR) and the test specimen retrofitted with the NBSD-based WSCS (PD-NBSD) were subjected to pseudo-dynamic testing and then tested for any cracks and breakage. Moreover, the resultant load-displacement curves (restoring force), temporal hysteresis loops with respect to the displacement, and maximum seismic response were analyzed to determine and compare the seismic retrofitting effect of PD-FR and PD-NBSD.

4.5.1. Crack and Failure Morphology

(1) PD-FR (with no reinforcement applied)

Figures 14 and 15 show the crack and failure patterns of the test frame with no reinforcement applied (PD-FR) when subjected to an input seismic ground motion of 200 cm/s^2. In PD-FR, initial flexural cracks started to occur at the lower part of the columns at 2.08 s (18.2 mm), as shown in these figures. Subsequently, at 2.4 s (18.2 mm), these flexural cracks expanded while shear cracks started to occur at both the upper and lower parts of the columns. At 2.89 s (38.9 mm), the shear cracks at the lower part of the column started to increase in width, and severe concrete delamination occurred. At 3.46 s (70.2 mm), these shear cracks significantly increased in width, where the maximum displacement occurred. Finally, a shear failure occurred at the lower part of the first floor of the test frame, which then led to the collapse of the frame.

This result was consistent with a previous study [46], which reported that school buildings with non-seismic details may be subject to large-scale seismic damage when an earthquake with a magnitude of 200 cm/s^2 occurred. These data are considered important evidence to demonstrate the necessity of applying seismic retrofitting to school buildings with non-seismic details of the 1980s.

(2) PD-NBSD-WSCS (retrofitted with NBSD)

Figures 16–18 show the crack and failure patterns of the test frame retrofitted with NBSD (PD-NBSD-WSCS) when subjected to an input seismic ground motion of 200, 300, and 400 cm/s^2, respectively. Figure 19 presents the crack patterns of the frame for each input seismic ground motion at the final stage.

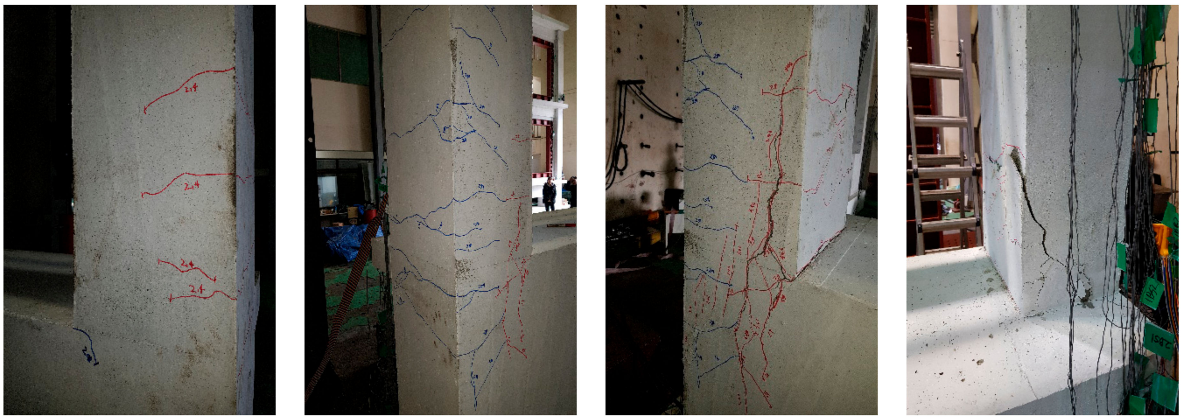

(**a**) (**b**) (**c**) (**d**)

Figure 14. Cracks and ultimate failure of test frame with no reinforcement applied (PD-FR) (200 cm/s^2): (**a**) flexural cracks at around 2.4 s (18.2 mm), (**b**) flexural and shear cracks at around 2.89 s (38.9 mm), (**c**) shear cracks and maximum displacement at around 3.46 s (70.2 mm), and (**d**) shear failure and maximum displacement at the final stage of the test.

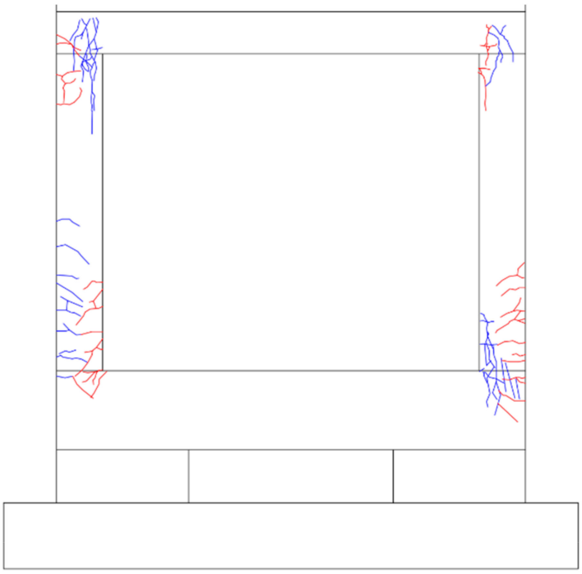

Figure 15. Cracks of test frame with no reinforcement applied (PD-FR) at the final stage (200 cm/s^2).

In this test frame retrofitted with NBSD (PD-NBSD-WSCS), fine initial flexural cracks started to occur at the lower part of the columns at around 1.88 s (3.5 mm) when the input seismic ground motion was set to 200 cm/s^2 (Figures 16 and 19a). Subsequently, at 2.61 s (12.7 mm), these flexural cracks increased in number, but their size remained limited. At 6.33 s (23.9 mm), where the maximum seismic response occurred, fine flexural cracks also occurred. The pseudo-dynamic testing was conducted for a period of 10 s. The results showed that PD-NBSD retrofitted with NBSD was subject to only fine flexural cracks in contrast to PD-FR with no reinforcement applied, which underwent a shear failure, when the input seismic ground motion was 200 cm/s^2.

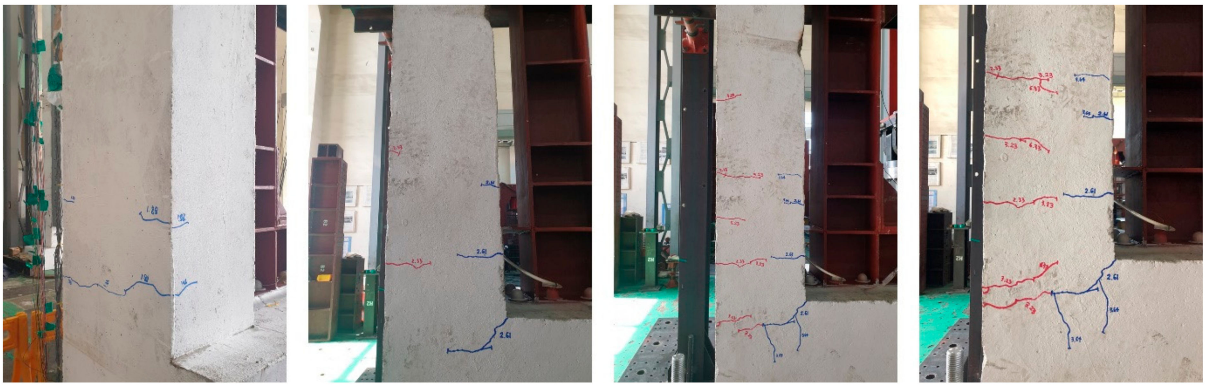

(**a**) (**b**) (**c**) (**d**)

Figure 16. Cracks and ultimate state of test frame retrofitted with NBSD-WSCS (PD-NBSD-WSCS) (200 cm/s^2): (**a**) flexural cracks at around 1.88 s (3.5 mm), (**b**) flexural cracks at around 2.61 s (12.7 mm), (**c**) flexural cracks at around 6.33 s (23.9 mm), and (**d**) patterns at the final stage (10 s).

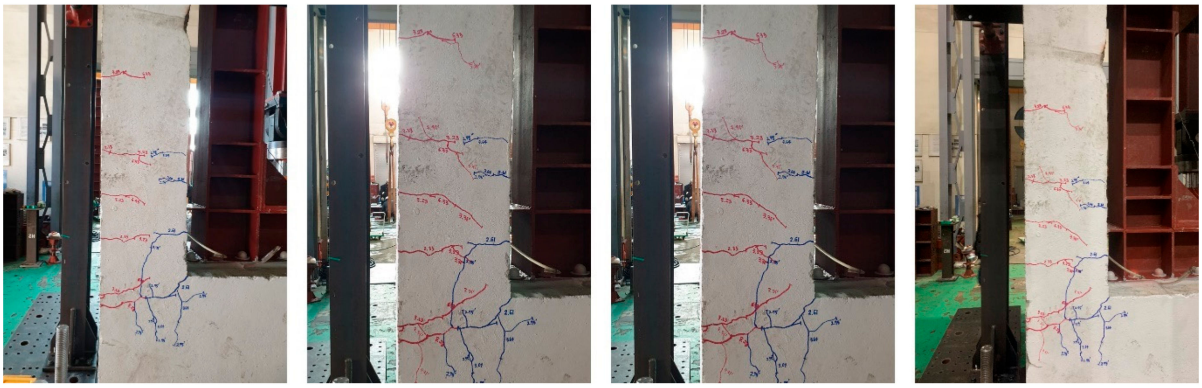

(**a**) (**b**) (**c**) (**d**)

Figure 17. Cracks and ultimate state of test frame retrofitted with NBSD-WSCS (PD-NBSD-WSCS) (300 cm/s^2): (**a**) flexural and shear cracks at around 2.75 s (37 mm), (**b**) flexural and shear cracks at around 3.31 s (46.6 mm), (**c**) flexural and shear cracks at around 3.7 s (49 mm), and (**d**) patterns at the final stage (10 s).

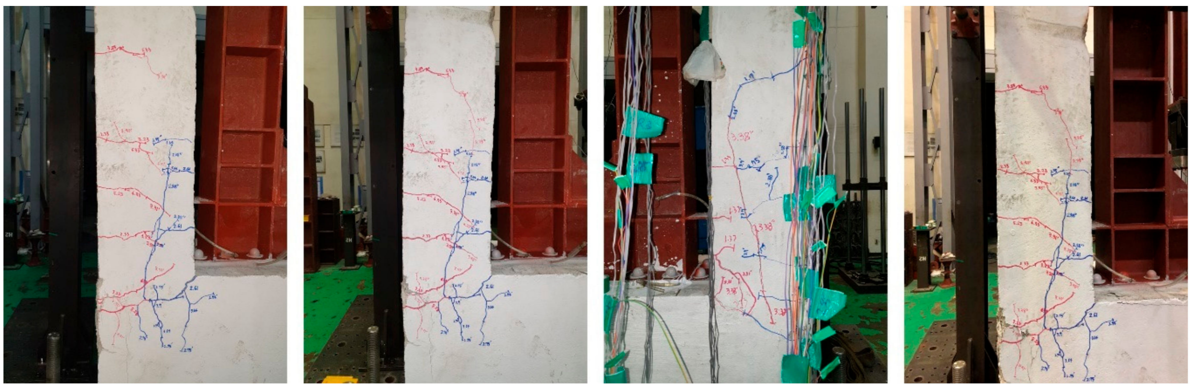

(**a**) (**b**) (**c**) (**d**)

Figure 18. Cracks and ultimate state of test frame retrofitted with NBSD-WSCS (PD-NBSD-WSCS) (400 cm/s^2): (**a**) flexural and shear cracks at around 2.88 s (75.1 mm), (**b**) flexural and shear cracks at around 3.38 s (85.2 mm), (**c**) flexural and shear cracks at around 3.7 s (85.6 mm), and (**d**) patterns at the final stage (10 s).

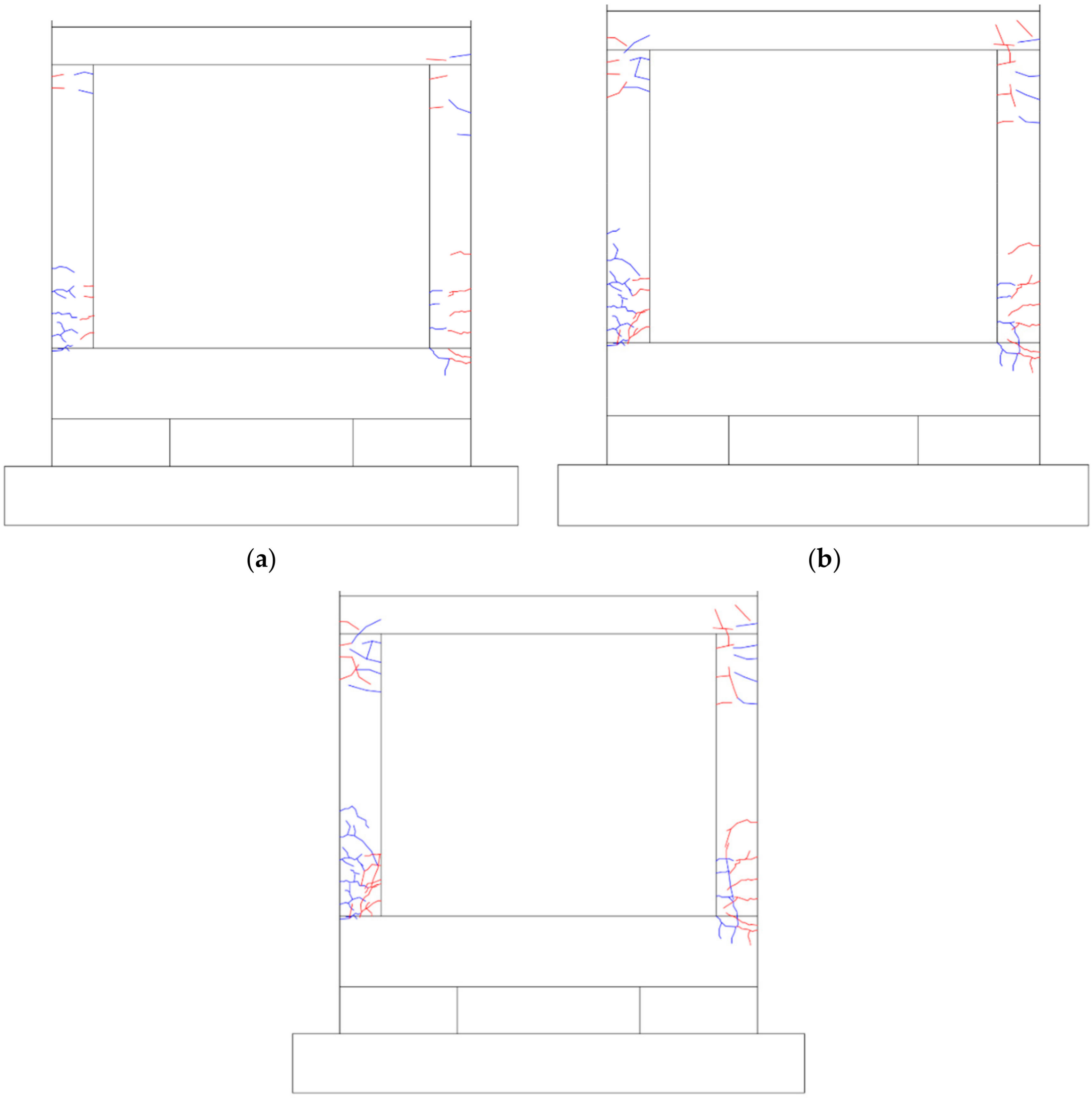

(**a**) (**b**) (**c**)

Figure 19. Cracks of test frame retrofitted with NBSD-WSCS (PD-NBSD-WSCS) at the final stage of the test; (**a**) 200 cm/s^2; (**b**) 300 cm/s^2; (**c**) 400 cm/s^2.

When the input seismic ground motion was increased to 300 cm/s^2 (Figures 17 and 19b), the number of flexural cracks was larger at 2.75 s (37.0 mm) compared to when the input seismic ground motion was 200 cm/s^2. From 3.7 s (49.0 mm) on, where the maximum seismic response occurred, small flexural cracks continued to occur, and it was found that these flexural cracks determined the failure mode of the frame. In the test frame with no reinforcement applied, as shown in Figures 14 and 15 above, a typical shear failure was observed, but PD-NBSD developed in the present study was found to undergo flexural failure; the failure mode shifted from shear to flexural.

When the input seismic ground motion was set to 400 cm/s^2, which simulated the occurrence of a large-scale earthquake, as shown in Figures 18 and 19c, more flexural cracks were observed at 2.88 s (75.1 mm) compared to when the input seismic ground motion was 300 cm/s^2, and, at the same time, shear cracks occurred but to a limited extent. At 3.38 s (85.2 mm), where the maximum seismic response occurred, both flexural and shear cracks increased in width and number, and the ultimate failure mode was determined by flexural shear cracks.

4.5.2. Maximum Seismic Response Load and Displacement

The test frame with no reinforcement applied (PD-FR) was subjected to pseudo-dynamic testing at an input seismic ground motion of 200 cm/s^2; the test frame retrofitted with NBSD-WSCS (PD-NBSD-WSCS) was subjected to pseudo-dynamic testing at input seismic ground motions of 200, 300, 400, and 500 cm/s^2, and the measured maximum response load and displacement were compared with respect to the failure mode and seismic damage, as shown in Table 9. In the test frame with no reinforcement applied, i.e., PD-FR, the maximum seismic response occurred at 272.5 kN with a displacement of 70.2 mm when the input seismic ground motion was 200 cm/s^2. At around 3.5 s, where the maximum seismic response occurred, the test frame finally underwent shear failure. Here, the degree of seismic damage was considered to correspond to *Collapse* in accordance with JBDPA [47] and Maeda et al. [48].

Table 9. Maximum response load-displacement and the degree of seismic damage.

Specimen Name	Input Seismic Ground Motion	Input Seismic Ground Motion (cm/s^2)	Maximum Load V_u (kN)	Maximum Displacement δ_u (mm)	Degree of Seismic Damage * (Failure Mode)
PD-FR	Hachinohe (EW)	200	272.5	70.2	Collapse (shear failure)
PD-NBSD-WSCS		200	419.5	23.8	Small (flexural cracks)
		300	592.9	46.6	Moderate (flexural shear cracks)
		400	711.9	85.6	Large (flexural shear failure)

* The degree of seismic damage was determined in accordance with JBDPA [46] and Maeda et al. [47].

In the test frame retrofitted with the NBSD system (PD-NBSD), the maximum seismic response occurred at 419.5 kN with a displacement of 23.8 mm when the input seismic ground motion was 200 cm/s^2. The degree of seismic damage was insignificant compared to PD-FR at the same seismic ground motion. At 300 cm/s^2, the maximum seismic response occurred at 592.9 kN with a displacement of 46.6 mm, and the corresponding degree of seismic damage was determined to be *Small* in accordance with JBDPA [47] and Maeda et al. [48].

These results confirmed that, given that the test frame with no reinforcement applied underwent shear failure, the reinforcement using NBSD led to a failure mode shift from shear to flexural failure, demonstrating the significantly improved energy dissipation capacity of the NBSD-based seismic control system developed in the present study. When the input seismic ground motion was 400 cm/s^2, i.e., when a large-scale earthquake was assumed, the maximum seismic response occurred at a shear stress of 711.9 kN with a displacement of 85.6 mm, the corresponding degree of seismic damage was determined to be *Large*. These results verify the seismic retrofitting performance of the NBSD-based seismic control system even when a large-scale earthquake with a recurrence period of 2400 years occurs.

4.5.3. Comparison and Analysis of the Load-Displacement Relationship and Displacement-Time Hysteresis

Figure 20 presents the load-displacement curves of the test frame retrofitted with NBSD (PD-NBSD-WSCS) at 200, 300, and 400 cm/s^2, along with the load-displacement curves obtained from the test frame with no reinforcement applied (PD-FR) at 200 cm/s^2 for comparison. Figure 21 shows the seismic response displacement-time hysteresis curves of the test frame retrofitted with NBSD (PD-NBSD-WSCS) at 200, 300, and 400 cm/s^2, along with the curves obtained from the test frame with no reinforcement applied (PD-FR) at 200 cm/s^2 for comparison. Based on these results, both their seismic response strength ratios and displacement ratios, which are important parameters for seismic performance evaluation, were estimated and compared, as summarized in Table 10.

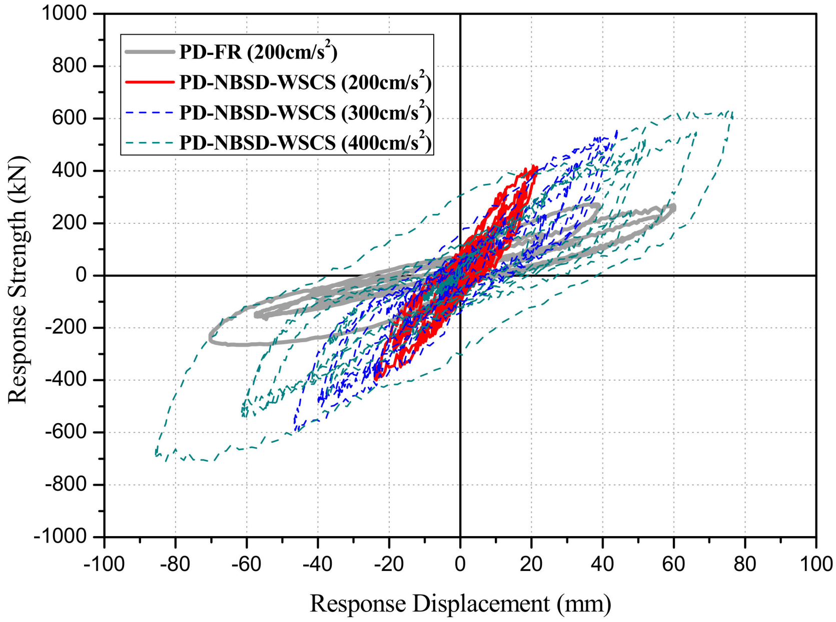

Figure 20. Comparison of seismic response shear stress–displacement curves.

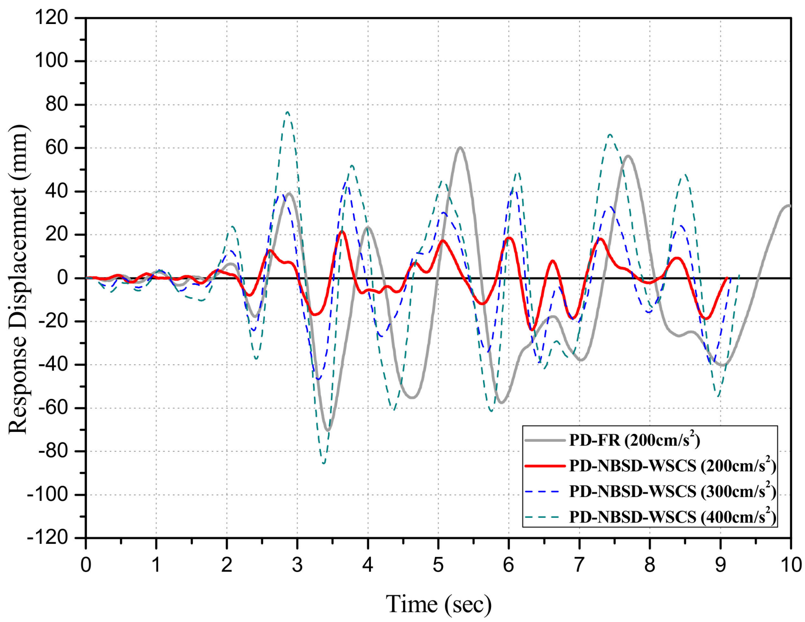

Figure 21. Comparison of seismic response shear stress–displacement curves.

The test frame retrofitted with the NBSD system exhibited seismic response strength about 1.53 times higher than the reference test frame (PD-FR) when the same input seismic ground motion was applied at 200 cm/s^2. The difference was even larger when the input seismic ground motion was higher: about 2.17 times at 300 cm/s^2 and about 2.61 times at 400 cm/s^2, as shown in the figures and table above. These results were also highly consistent with the ultimate failure patterns shown in Figures 14–19. The measured seismic response displacement was about 0.33 times higher at 200 cm/s^2, 0.66 times higher at 300 cm/s^2, and 1.21 times higher at 400 cm/s^2 in the test frame retrofitted with the NBSD system than in the reference frame, respectively. When the same input seismic ground motion was applied (200 cm/s^2), the seismic response displacement was about 67% smaller, indicating that the NBSD-based seismic retrofitting method proposed in the present study proved to be highly effective in improving the seismic energy absorption capacity of the system.

Table 10. Comparison of seismic response strength ratios and displacement ratios.

Specimen Name	Input Seismic Ground Motion	Degree of Acceleration (cm/s^2)	Seismic Response Load		Seismic Response Displacement	
			Maximum Load V_u (kN)	Maximum Strength Ratios R_s *1	Maximum Displacement δ_u (mm)	Displacement Ratios Rd *2
PD-FR	Hachinohe (EW)	200	272.5	1.00 (272.5/272.5)	70.2	1.00 (70.2/70.2)
PD-NBSD-WSCS	Hachinohe (EW)	200	419.5	1.53 (419.5/272.5)	23.8	0.33 (23.8/70.2)
		300	592.9	2.17 (592.9/272.5)	46.6	0.66 (46.6/70.2)
		400	711.9	2.61 (592.9/272.5)	85.6	1.21 (46.6/70.2)

*1 R_s: ratio of maximum strength between NBSD-WSCS and reference specimens; *2 R_d: ratio of maximum displacement between NBSD-WSCS and reference specimens.

5. Comparison of the Pseudo-Dynamic Test Results and Nonlinear Dynamic Analysis Results

Based on the NBSD material test and pseudo-dynamic test results, described in Sections 3 and 4, the restoring force characteristics of beams, columns, and reinforcing members (NBSD) were proposed to implement nonlinear dynamic analysis of the full-size two-story test frame retrofitted with the NBSD seismic retrofitting method. The proposed restoring force characteristics were used to conduct nonlinear dynamic analysis of the two-story pseudo-dynamic test frame, and the results were then compared with the pseudo-dynamic test results.

5.1. Overview of the Nonlinear Dynamic Analysis

Nonlinear dynamic analysis was conducted on both the full-size two-story RC frame with no reinforcement applied and the test frame retrofitted with the NBSD system shown in Figure 11 in Section 4.4. In reality, actual structures vibrate in a three-dimensional and complex manner, but, in the present study, it was assumed that the used columns, beams, and walls were wire-type materials so that the test frame was modeled as a plane frame, in which only the seismic force in the horizontal direction was considered. The floor-specific structural evaluation was conducted at the member level, and the following assumptions were applied in the analysis: (1) The position of each member's yield hinges was determined based on references [7,39], and the segment from the center of each member, including column and beam joints, to the ends of the members, where yield hinges occur, should be assumed to be rigid. (2) The strength of a beam should be determined considering the effect of the slab reinforcing bars present within the effective width of the slabs that collaborate with the corresponding beam.

Each member should be modeled to allow flexural springs, shear springs, and axial springs to be serially connected, as shown in Figure 22a. The modified Ramberg-Osgood (MRO) model was employed as a hysteresis model for the NBSD-based seismic control system because the model is suitable to simulate the hysteric behavior of steel slit dampers. The hysteric characteristics of the MRO model with respect to the stiffness can be represented by the primary stiffness ($\alpha \cdot K_0$) and secondary stiffness ($\beta \cdot K_0$), which can be obtained by applying the stiffness coefficient (α, β) to the initial stiffness (K_0). The unloading and reloading hysteresis loops were characterized based on the curve number (λd). Table 11 summarizes the parameters used in the MRO model for the NBSD system. The nonlinear analysis results obtained based on Table 11 were then compared with the NBSD material test results obtained during the cyclic loading tests described in Section 4, as shown in Figure 23. The results showed that the simulated hysteric behavior was largely consistent with the experimental results, except that the energy dissipation exhibited an error of about 1%.

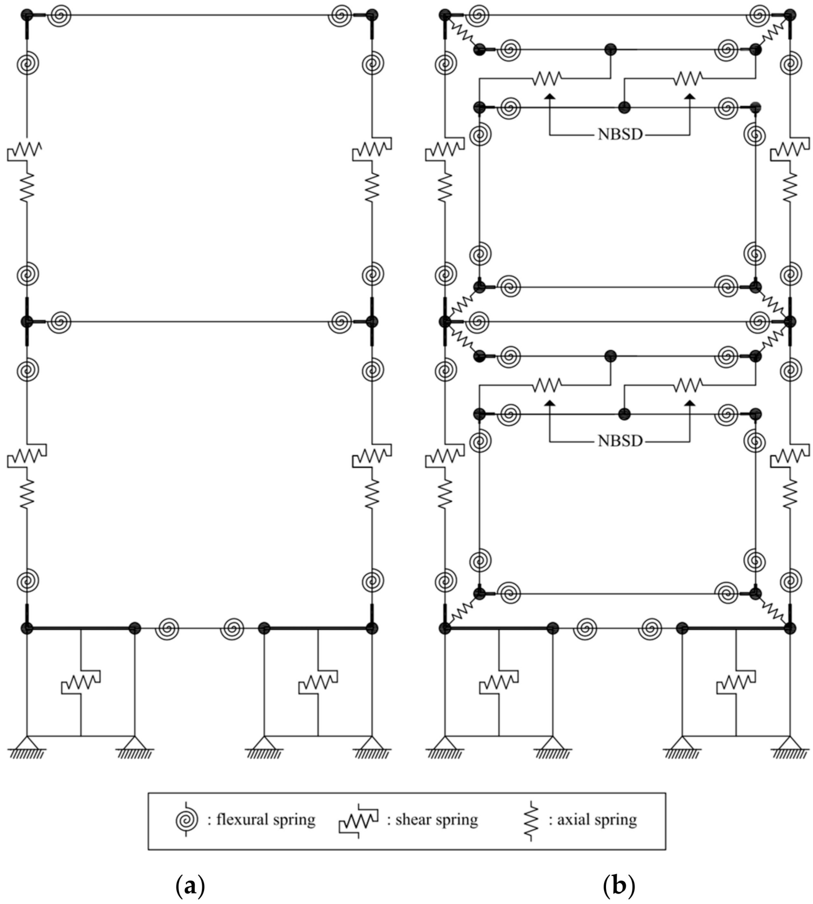

Figure 22. Nonlinear dynamic analysis models: (**a**) Existing frame with no reinforcement applied (PD-FR) and (**b**) frame retrofitted with NBSD-WSCS (PD-NBSD-WSCS).

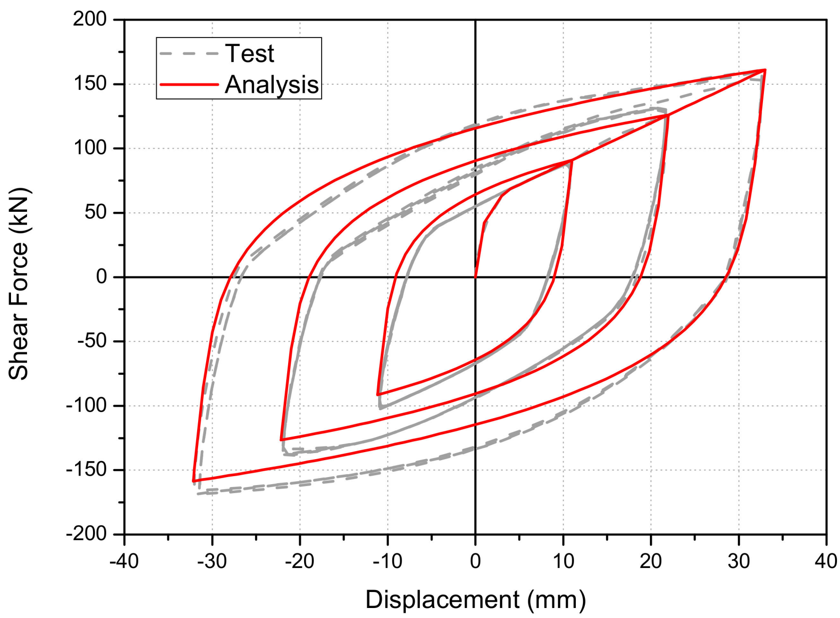

Figure 23. Comparison of the nonlinear analysis and material test results of NBSD.

Table 11. Parameters used in the modified Ramberg-Osgood (MRO) model for the NBSD system.

Test Specimen	K_o,K'_o (kN/mm)	Q_o,Q'_o (kN)	α,α'	Q_y,Q'_y (kN)	β,β'	λ_d	Energy Dissipation [Test] (kN·m)	Energy Dissipation [Analysis] (kN·m)	Error Rate [Test/Analysis] (%)
NBSD	65.1	37.8	0.161	66.4	0.056	5.0	119.5	118.3	1.01 [119.5/118.3]

K_o, K'_o: initial stiffness, Q_o, Q'_o: cracking strength, α, α': primary stiffness coefficient, Q_y, Q'_y: yield strength, β, β': secondary stiffness coefficient, and λ_d: curve number (unloading-reloading curve area).

The restoring force characteristics of columns with non-seismic details subject to shear failure (shear spring) were proposed based on applicable domestic columns with non-seismic details and then determined using Equation (10) [49] below.

$$Q_u = 2.5Q_c \ ; \ \delta_u = 5.0\delta_c \tag{10}$$

Here, Q_u: ultimate stress at shear failure, Q_c: stress at shear cracks, δ_u: displacement at shear failure, and δ_c: displacement at shear cracks.

The test frame with no reinforcement applied also includes ground beams and walls on the foundation level. It is composed of a total of 12 nodal points, including two deck panels and branch points, as shown in Figure 22b. The test frame retrofitted with NBSD-WSCS (PD-NBSD) includes nodal points in which the existing RC frame with added steel frames, as well as the NBSD system and the members that are used to mount the NBSD system, as shown in Figure 22b. Thus, it is composed of a total of 28 nodal points, including branch points. Joints in which the existing RC members are connected with steel frames were modeled using link-joint elements.

Nonlinear dynamic analysis was performed using CANNY, a commercial software package developed by Li [50] to implement the three-dimensional nonlinear dynamic analysis. Table 12 presents an overview of the restoring force characteristics of each member used in the nonlinear dynamic analysis.

Table 12. Restoring force characteristics of each member used in the nonlinear dynamic analysis.

Member	Restoring Force Model		Model Name
Beam	Flexural spring	CP3	Cross-peak trilinear model
	Shear spring	OO3	Trilinear origin-oriented
Column	Flexural spring	CA7	CANNY sophisticated trilinear hysteresis model
	Shear spring	OO3	Trilinear origin-oriented
	Axial spring	AE1	Axial stiffness model
Wall	Shear spring	OO3	Trilinear origin-oriented
Anchor bolt	Shear spring	EL2	Bilinear elastic model
NBSD	Damper spring	RO3	Modified Ramberg-Osgood model
Steel frame (H-beam)	Flexural spring	BL2	Degrading bilinear model
	Shear spring	EL1	Linear elastic model

5.2. Comparison of the Nonlinear Dynamic Analysis and Pseudo-Dynamic Test Results

Nonlinear dynamic analysis was performed using the Hachinohe wave (EW) at 200 and 300 cm/s^2 applied in the pseudo-dynamic tests. Moreover, the model described in Section 5.1, along with CANNY [50] was employed. As mentioned earlier, 200 cm/s^2 of the Hachinohe wave (EW) was applied to the pseudo-dynamic testing of the test frame with no reinforcement, while 200 and 300 cm/s^2 were applied to the test frame retrofitted with NBSD.

Figure 24 shows the seismic response load-displacement and time-displacement hysteresis loops obtained from the first floor of the test frame with no reinforcement applied during nonlinear dynamic analysis and pseudo-dynamic tests when the input seismic ground motion was 200 cm/s^2. Figures 25 and 26 show the seismic response load-displacement and time-displacement hysteresis loops obtained from the first floor of the test frame retrofitted with the NBSD system during nonlinear dynamic analysis and pseudo-dynamic tests when the input seismic ground motion was 200 and 300 cm/s^2, respectively. Figure 27 shows the seismic response load-displacement relationships of NBSD during nonlinear dynamic analysis and pseudo-dynamic tests at 200 and 300 cm/s^2. Table 13 compares the maximum response load-displacement relationship between the nonlinear dynamic analysis and pseudo-dynamic tests.

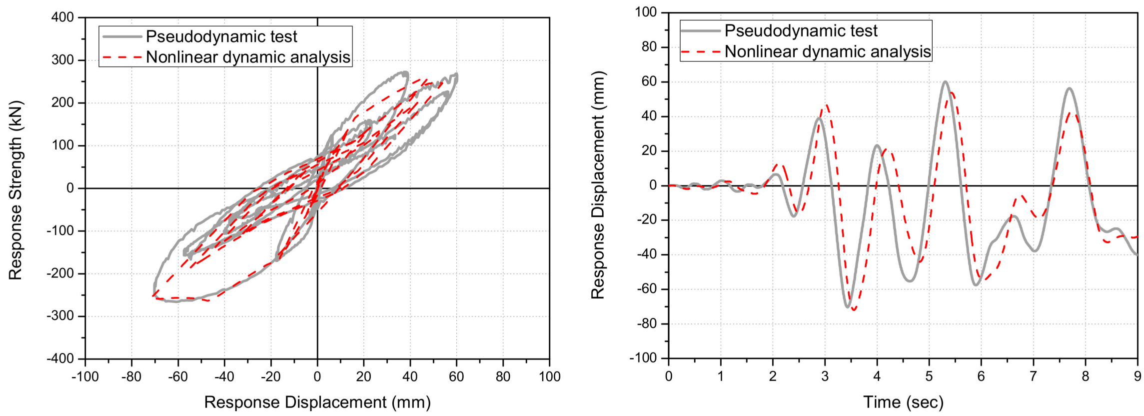

Figure 24. Comparison of seismic response load-displacement and displacement hysteresis loops during nonlinear dynamic analysis and pseudo-dynamic tests of the test frame with no reinforcement applied (first floor, 200 cm/s^2).

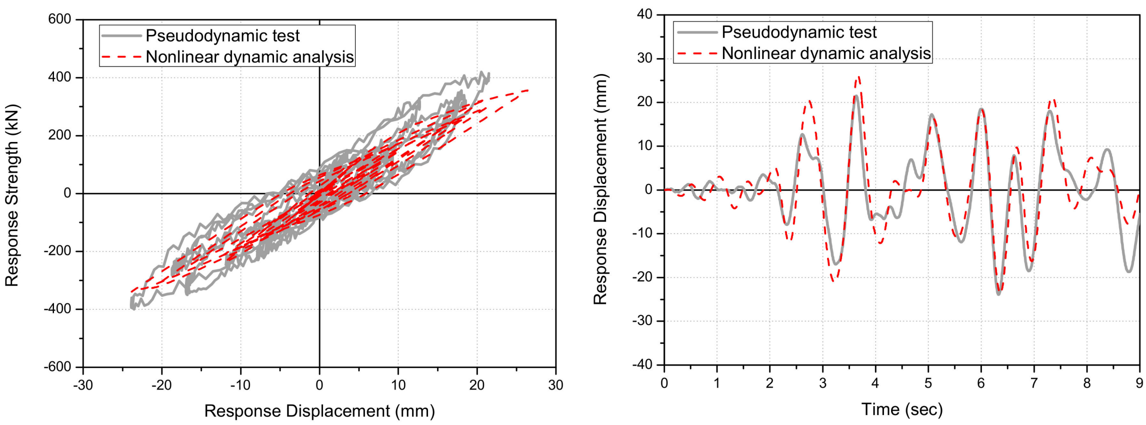

Figure 25. Comparison of seismic response load-displacement and displacement hysteresis loops during nonlinear dynamic analysis and pseudo-dynamic tests of the test frame retrofitted with NBSD-WSCS (first floor, 200 cm/s^2).

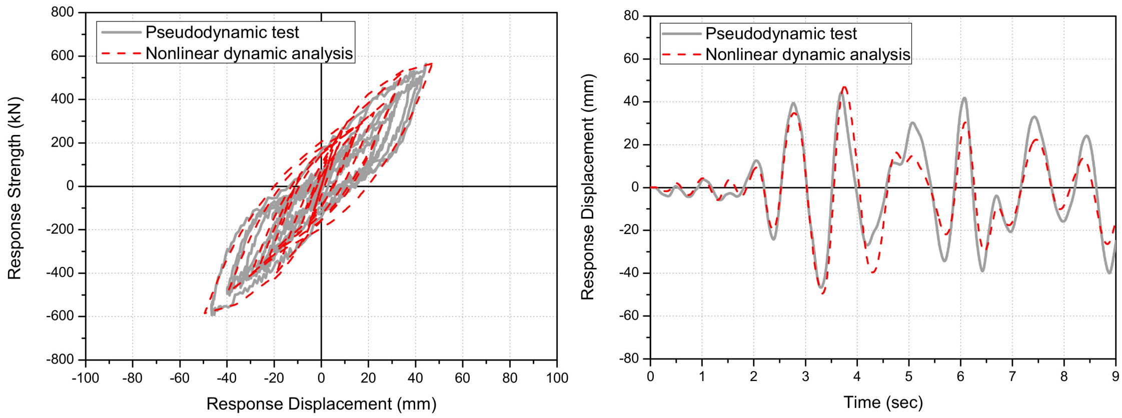

Figure 26. Comparison of seismic response load-displacement and displacement hysteresis loops during nonlinear dynamic analysis and pseudo-dynamic tests of the test frame retrofitted with NBSD-WSCS (first floor, 300 cm/s^2).

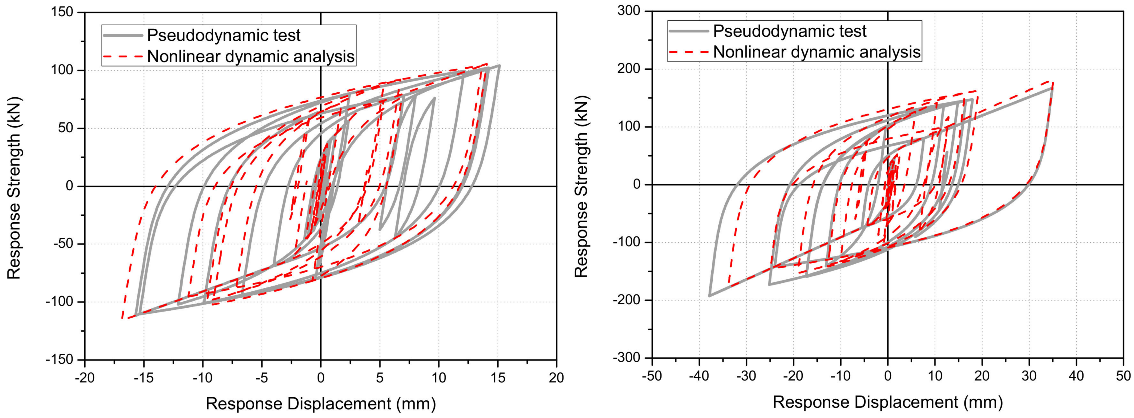

Figure 27. Comparison of seismic response load-displacement curves during nonlinear dynamic analysis and pseudo-dynamic tests of NBSD (first floor, 300 cm/s^2).

Table 13. Comparison of maximum response load-displacement relationship between nonlinear dynamic analysis and pseudo-dynamic test results.

Specimen Name	Input Seismic Acceleration (cm/s^2)	Method	Maximum Displacement (mm)	Maximum Displacement Deviation Ratio [Analytical/Experimental]	Maximum Load (kN)	Maximum Load Deviation Ratio [Analytical/Experimental]
PD-FR	200	Pseudo-dynamic testing	70.2	1.02	272.5	0.96
		Nonlinear dynamic analysis	71.9		263.0	
PD-NBSD-WSCS	200	Pseudo-dynamic testing	26.4	0.90	356.2	1.17
		Nonlinear dynamic analysis	23.9		419.5	
	300	Pseudo-dynamic testing	49.4	0.94	584.2	1.01
		Nonlinear dynamic analysis	46.6		592.9	

When the input seismic acceleration was 200 cm/s^2, the maximum seismic response load and displacement of the test frame with no reinforcement applied (PD-FR) were

263.0 kN and 71.9 mm, respectively, in the nonlinear dynamic analysis and 272.5 kN and 70.2 mm, respectively, in the pseudo-dynamic testing (Figure 24 and Table 13). When the input seismic acceleration was 200 cm/s^2, the maximum seismic response load and displacement of the test frame retrofitted with the NBSD system (PD-NBSD) were 419.5 kN and 23.9 mm, respectively, in the nonlinear dynamic analysis and 356.2 kN and 26.4 mm, respectively, in the pseudo-dynamic testing (Figure 25 and Table 13). At a seismic ground motion of 200 cm/s^2, the deviation between the nonlinear dynamic analysis and pseudo-dynamic test results was not significant at 10% or less on average. When the input seismic ground motion was 300 cm/s^2, the maximum seismic response load and displacement of PD-NBSD were 592.9 kN and 46.6 mm, respectively, in the nonlinear dynamic analysis and 584.2 kN and 49.4 mm, respectively, in the pseudo-dynamic testing (Figure 26 and Table 13). The two methods provided very similar results.

A similar level of deviation was observed in the seismic response load-displacement relationships obtained from both PD-NBSD and NBSD, as shown in Figure 27. These results confirmed that the nonlinear dynamic analysis model and methodology developed in the present study were able to effectively simulate the NBSD-based seismic retrofitting method and the seismic behavior of RC frames retrofitted with the NBSD system. This led to the conclusion that the seismic retrofitting performance of the NBSD-based system developed in the present study could be effectively evaluated via nonlinear dynamic analysis based on the analytical models and methods established in Section 5.1.

6. Seismic Performance Evaluation of RC Structures Retrofitted with the NBSD-Based Window-Type Seismic Control System

6.1. Overview of the Nonlinear Dynamic Analysis

The nonlinear analytical model and method established in Section 5 were found to be effective in simulating the seismic behavior of RC structures retrofitted with NBSD-WSCS. In an attempt to commercialize this NBSD-WSCS developed in the present study, nonlinear dynamic analysis was conducted on the entire RC building with non-seismic details retrofitted with the NBSD-WSCS (See Figure 10), as shown in Section 4.4, based on the analytical model and method established in Section 5.1. The seismic response load, displacement characteristics, and energy dissipation capacity of the test building were then examined before and after the reinforcement, and the energy dissipation capacity and seismic response load and displacement of the used dampers were evaluated to determine the seismic retrofitting performance of the developed system.

Nonlinear dynamic analysis was conducted using CANNY [50], a three-dimensional analysis program, as in Section 5, and earthquake levels used for seismic design of the target building were applied. The input seismic ground motion was set to 200 cm/s^2 using the Hachinohe wave (EW), under which the reference frame with no reinforcement applied underwent a collapse. Figure 28 shows the RC school building model before and after seismic strengthening, and the amount of seismic strengthening needed for the NBSD seismic control system was calculated by Equations (11)–(13). The equations were derived from the Newmark's equal energy criterion [51,52], which is the same method used by Japan to evaluate seismic energy absorption of seismic devices [7].

$$Q_{ydp} = \frac{\left[\left(\frac{E_{Ro}}{E_o}\right)^2 - 1\right]\cdot\phi^2\cdot(2\mu-1)\cdot\mu_{dp}}{2\beta\cdot\left(\mu\cdot\mu_{dp}-1\right)}\cdot Q_{yst} \quad (11)$$

$$E_{Ro} = C_{yst}\cdot\sqrt{\phi^2(2\mu-1) + 2\beta\cdot\alpha_c\left(\mu - \frac{1}{\mu_{dp}}\right)} \quad (12)$$

$$E_o = C_{yst}\cdot\sqrt{\phi^2(2\mu-1)} \quad (13)$$

Here, Q_{ydp}: required amount of seismic reinforcement for the damper (required stress), Q_{yst}: yield proof stress of existing structural members, E_{Ro}: basic seismic capacity index after the seismic reinforcement, E_o: basic seismic capacity index of existing structural members, ϕ : coefficient for ductility index calculation of the existing RC structure (=$1/0.75(1+0.05\mu)$), μ : ductility of the existing structure (=$\delta_{max}/\delta_{yst}$), μ_{dp} : damper ductility for yield displacement of the existing frame (=$\delta_{yst}/\delta_{ydp}$), δ_{yst}: yield displacement of the existing structure, δ_{ydp}: yield displacement of the damper, C_{yst}: Yield proof stress of the existing structure expressed as a shear stress coefficient (=Q_{yst}/W), β: energy dissipation ratio of the damper, α_c: yield proof stress of the damper (C_{ydp}), yield proof stress of the existing structure (C_{yst}), and the ratio of the two, i.e., the damper's yield proof stress ratio (=C_{ydp}/C_{yst}).

The same specifications of the damper as used in the tests and analytical models of Sections 3 and 5 were applied. Based on them, the seismic capacity requirements and the required number of dampers to meet the seismic reinforcement target were determined, as shown in Table 14. The basic seismic capacity index after seismic reinforcement (E_{Ro}) provided in Table 14 was determined based on a previous study [53] on the target seismic capacity of domestic RC structures with non-seismic details as follows: $E_{Ro} = 0.52$, considering the life safety (LS) target corresponding to the input seismic ground motion of 200 cm/s^2.

Table 14. Estimated amount of seismic reinforcement for the NBSD-based seismic control system.

Estimation of the Target Building's Seismic Performance						
Floor	Floor height (mm)	Weight of each floor W (kN)	Yield displacement δ_{yst} (mm)	Yield proof stress Q_{yst} (kN)	Failure mode	Basic seismic capacity index E_o
1	3300	1133.4	24.1	2779	Shear failure	0.24
2	3300	7556	27.9	2268	Shear failure	0.24
3	3300	3778	18.0	1343.7	Shear failure	0.23
Estimation of Required Amount of Reinforcement						
Damper's yield displacement *1 δ_{ydp} (mm)	Damper yield proof stress *2 (kN)	Cumulative plastic deformation ratio β	Target seismic capacity by Reinforcement *3 E_{Ro}	Required damper stress Q_{ydp}	Required number of dampers [EA]	Number of dampers applied [EA]
1.5	152.0	10	0.52	537.9	3.53	4
			0.52	445.7	2.93	4
			0.52	282.6	1.85	2

*1: This parameter refers to the yield displacement of the damper developed in the present study. It was set to an average of 1.5 mm, as shown in Table 2; *2: the yield proof stress of the damper refers to the stress of a single frame for seismic reinforcement. Thus, it was calculated based on Table 2 of Section 3, as follows: 76 kN × 2 EA = 152.0 kN; *3: this parameter was determined based on a previous study [36] on the target seismic capacity of domestic RC structures with non-seismic details, considering the life safety (LS) target corresponding to the input seismic ground motion of 200 cm/s^2.

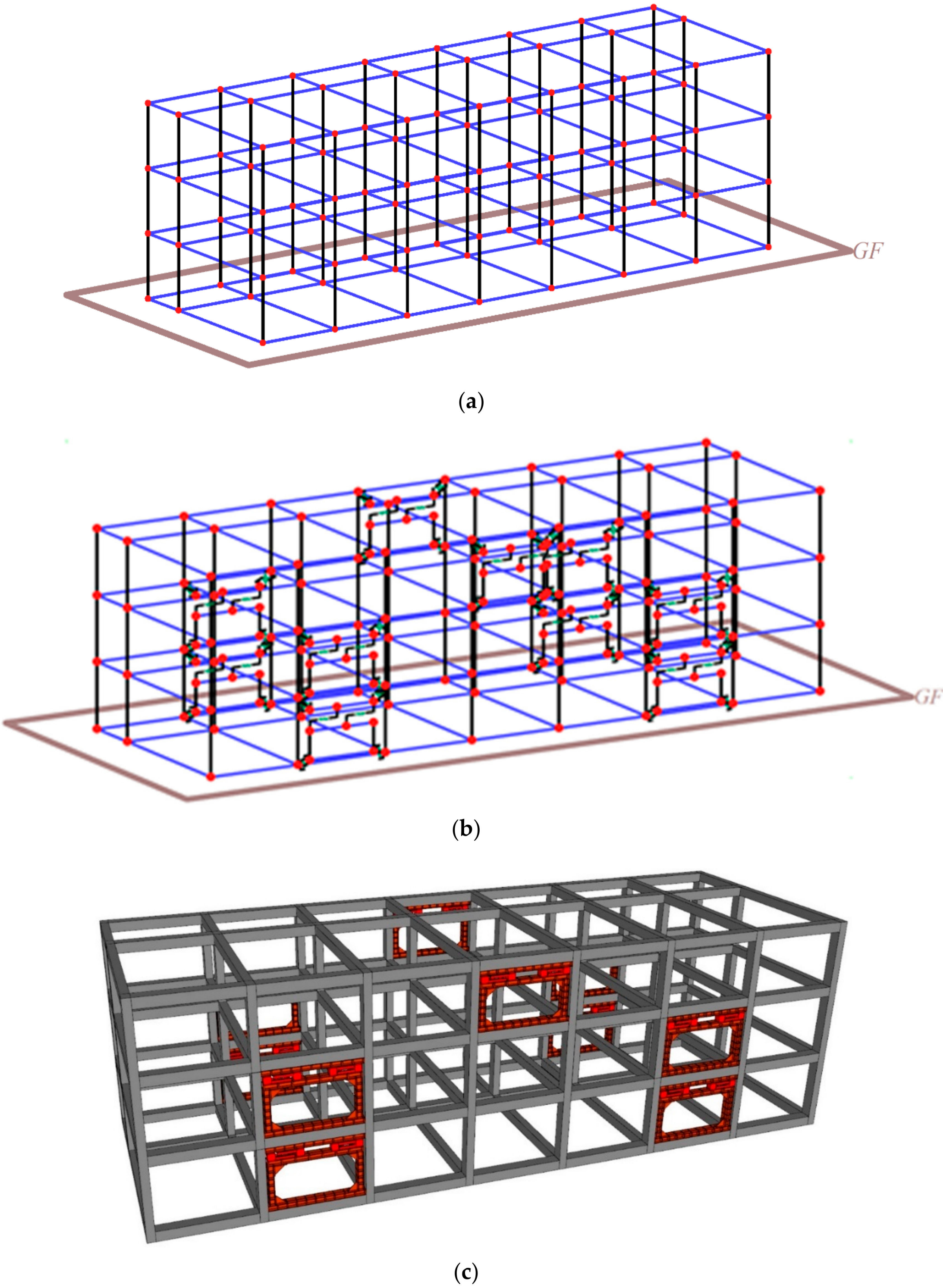

Figure 28. Analytical models and simulated frames of the target RC school building before and after reinforcement: (**a**) analytical model before seismic reinforcement, (**b**) analytical model after seismic reinforcement, and (**c**) simulated frame after seismic reinforcement.

6.2. Nonlinear Dynamic Analysis Results before and after Seismic Reinforcement

Nonlinear dynamic analysis before and after seismic reinforcement was conducted based on the analytical models described in Section 6.1. On the first floor of the test building with no reinforcement applied, shear cracks occurred at its column members at 2.1 s (3.9 mm) when the input seismic ground motion was 200 cm/s^2. Subsequently, the maximum seismic response occurred at 3584.2 kN at 3.3 s (49.1 mm), at which the test building finally collapsed. In the test building retrofitted with NBSD-WSCS, shear cracks occurred at its column members at 2.3 s (5.4 mm) when the input seismic ground motion was 200 cm/s^2. Following the maximum seismic response at 3.6 s (17 mm), however, seismic responses remained lower than the maximum level, leading to limited seismic damage.

The floor-specific load-displacement curves and time-displacement hysteresis loops of both the test building with no reinforcement applied and the test building retrofitted with NBSD-WSCS were obtained and compared, as shown in Figures 29 and 30. Among these analytical results, the maximum response stress and displacement of the two test buildings at 200 cm/s^2, which are important parameters for seismic performance evaluation, were compared, as summarized in Table 15. As can be seen in the figures and table above, at 200 cm/s^2, the maximum seismic response displacement of the test building retrofitted with NBSD-WSCS was about 0.35 times on the first floor, 0.37 times on the second floor, and 0.42 times on the third floor that of the test building with no reinforcement applied, respectively.

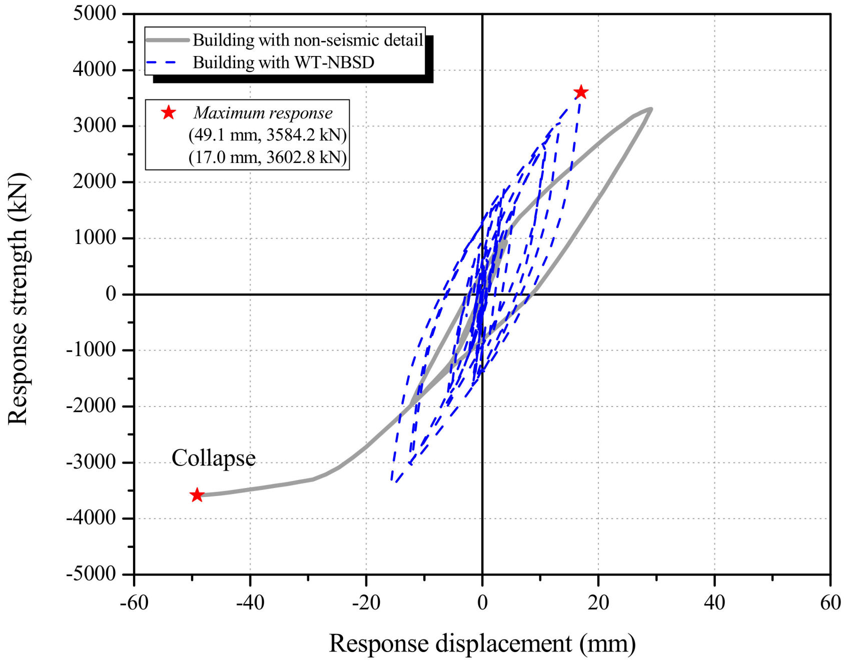

Figure 29. Seismic response load-displacement curves of the reference building and the building retrofitted with NBSD (firsts floor).

Table 15. Comparison of the maximum seismic response and damage before and after reinforcement.

Building	Floor	Maximum Response Stress V_{max} (kN)	Maximum Response Displacement δ_{max} (mm)	Failure Mode or Crack Patterns	Degree of Seismic Damage
No reinforcement applied	1	3584.2	49.1	Shear failure	Collapse
	2	2651.9	38.2	Shear failure	Large
	3	1411.3	22.6	Shear cracks	Small
Retrofitted with NBSD	1	3602.8	17.0	Flexural/shear cracks	Small
	2	2951.6	14.3	Flexural/shear cracks	Small
	3	1627.1	9.5	Flexural cracks	Insignificant

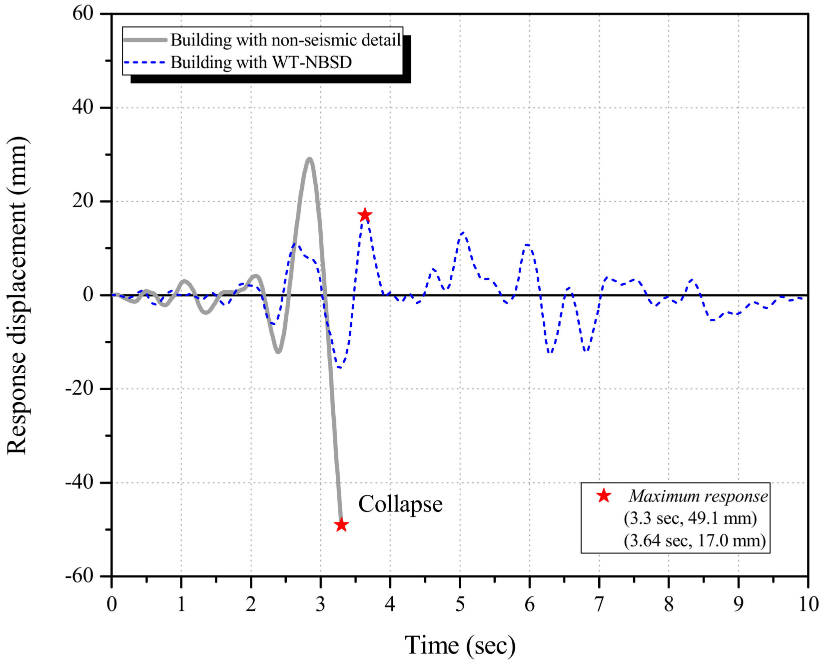

Figure 30. Time-displacement hysteresis loops of the reference building and the building retrofitted with NBSD (firsts floor).

These results confirmed the effectiveness of the seismic retrofitting design and NBSD-based seismic reinforcement method proposed in the present study. Figure 31 shows the seismic load-displacement response relationship obtained from the first floor of the test building retrofitted with NBSD-WSCS, and Table 16 summarizes the contributions of NBSD to energy dissipation with respect to the earthquake input. This clearly indicated that NBSD-WSCS with excellent energy dissipation capacity was able to accommodate about 42% of the total energy exerted on the test building.

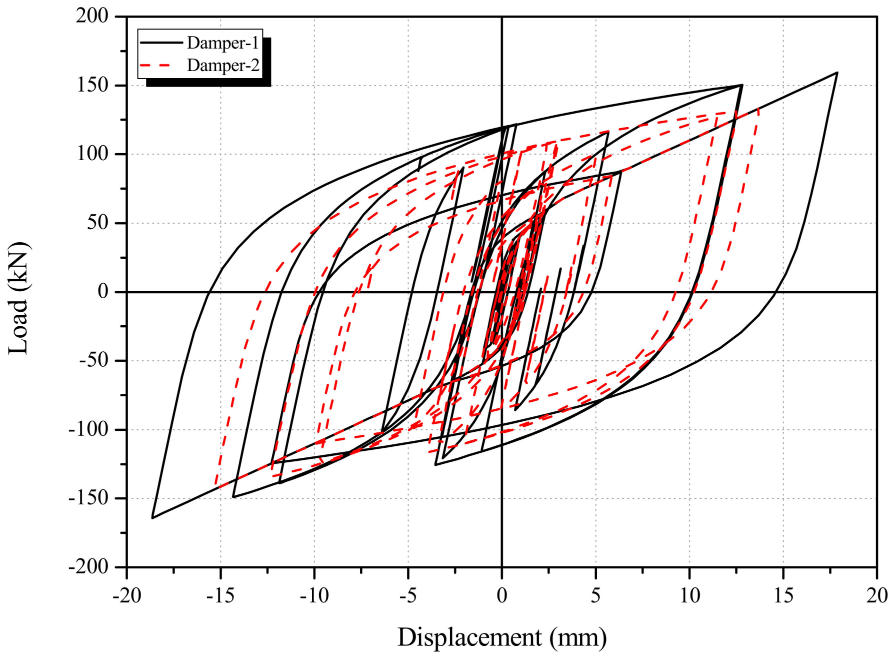

Figure 31. Seismic response load–displacement relationship of NBSD.

Table 16. Contribution of the NBSD seismic control system to seismic response energy dissipation (total).

Building	Kinetic Energy E_K (kN·m)	Plastic Deformation Energy E_S (kN·m)	Damping Energy E_D (kN·m)	Total Energy E	Plastic Deformation Energy of NBSD-WSCS (kN·m)	Contribution of NBSD-WSCS (%)
NBSD-WSCS	0.1	328.1	28.5	357.0	149.5	41.8

The shear ductility (μ_s) of the column members on each floor of both the test building with no reinforcement applied and the test building retrofitted with NBSD-WSCS is presented in Figures 32 and 33. Here, the shear ductility (μ_s) was defined as the ratio of the maximum seismic response shear displacement (δ_{max}) to the displacement when shear cracks occur (δ_c), i.e., $\mu_s = \delta_{max}/\delta_c$. $\mu_s = 5_s = 5$ refers to the moment when a shear failure occurs.

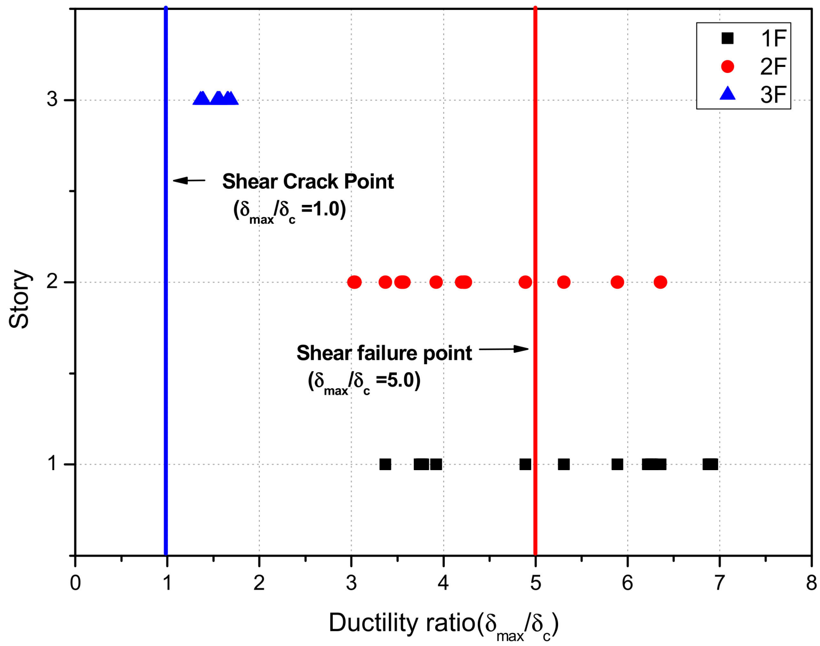

Figure 32. Shear ductility of all column members determined via nonlinear dynamic analysis of the reference building.

As shown in Figure 32, on the first floor of the reference building with non-seismic details, 15 out of the 24 columns were subject to shear failure. On the second floor, shear failure occurred at three columns. In contrast, on the first floor of the test building retrofitted with NBSD-WSCS, only shear cracks with μ_s = 3 or less occurred at the columns, and it was found that no column members exceeded the criteria for shear failure. According to previous studies [47,48], the degree of seismic damage observed in the reference building was considered to correspond to *Collapse*, while that observed in the building retrofitted with NBSD-WSCS was considered to be *Small*. These results showed that the building retrofitted with NBSD-WSCS was able to meet the target life safety (LS) for the seismic load of 200 cm/s^2, as defined in Section 6.1, and this seismic retrofitting method using NBSD-WSCS is a novel approach that has a high potential for commercialization.

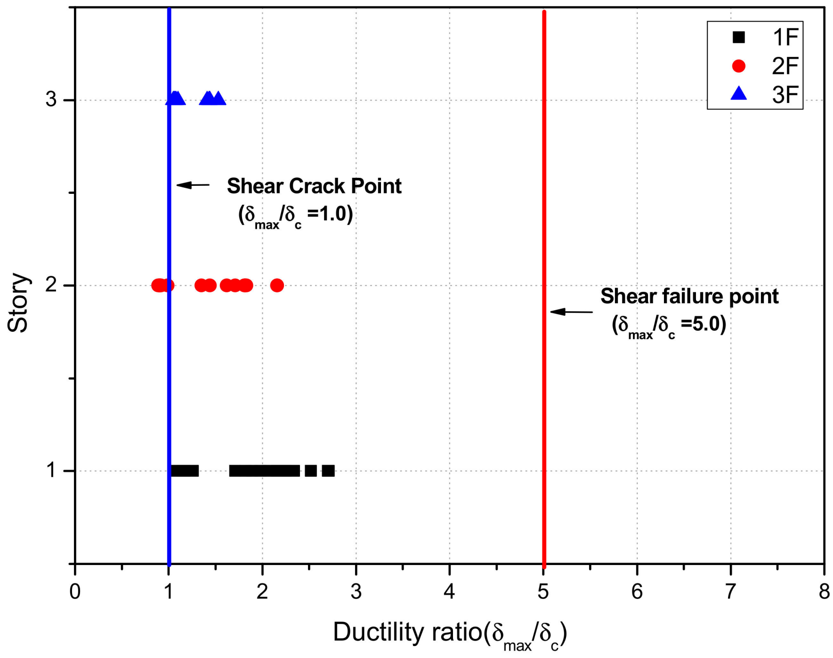

Figure 33. Shear ductility of all column members determined via nonlinear dynamic analysis of the building retrofitted with NBSD-WSCS.

7. Conclusions

In the present study, a window-type seismic control system (WSCS) using non-buckling slit dampers (NBSDs) was proposed and developed. Materials testing was also conducted to examine the material performance and energy dissipation capacity of the steel NBSD system. A full-scale two-story frame structure modeled from existing RC structures with non-seismic details was subjected to pseudo-dynamic testing. The seismic retrofitting performance of NBSD-WSCS, when applied to existing RC structures, was examined and verified, and based on the pseudo-dynamic testing results, a restoring force characteristics model was proposed. Further, based on the proposed restoring force characteristics, nonlinear dynamic analysis was conducted, and the results were compared with those obtained by the pseudo-dynamic tests. Finally, nonlinear dynamic analysis was conducted on the entire RC building with non-seismic details retrofitted with NBSD-WSCS. The major findings of the present study are as follows.

(1) Cyclic loading tests were conducted according to the test method for displacement-controlled seismic control systems provided in KDS 41 [12] to check NBSD-WSCS for conformity with the seismic performance requirements. The results confirmed that the NBSD-based test specimen provided adequate performance as a displacement-controlled seismic control system.

(2) Pseudo-dynamic testing was conducted at seismic intensity of 200 cm/s^2. The results showed that the full-size two-story RC test frame with no reinforcement applied underwent shear failure, while only minor seismic damage was expected for the test frame retrofitted with NBSD-WSCS. Even when the seismic intensity was set to 300 cm/s^2, only small or moderate seismic damage was expected. These results confirmed that, given that the test frame with no reinforcement applied underwent shear failure, the reinforcement using NBSD led to a failure mode shift from shear to flexural failure, demonstrating the significantly improved energy dissipation capacity of NBSD-WSCS developed in the present study.

(3) In addition, based on material testing and pseudo-dynamic test results obtained from NBSD members, the characteristics of beams, columns, and reinforcing members (NBSD) with respect to restoring force were proposed to implement the nonlinear dynamic analysis of the full-size two-story test frame retrofitted with NBSD-WSCS.

Further, based on the proposed restoring force characteristics, nonlinear dynamic analysis was conducted, and the results were compared with those obtained by the pseudo-dynamic tests. It was then found that the average deviation ratios in seismic response load and displacement were within 10%, i.e., the two methods provided similar results. This further confirmed that the nonlinear dynamic analysis model and methodology developed in the present study were able to effectively simulate and evaluate the seismic retrofitting performance of this novel NBSD-based WSCS via nonlinear dynamic analysis.

(4) In an attempt to commercialize this NBSD-based WSCS, nonlinear dynamic analysis was conducted on the entire RC building with non-seismic details retrofitted with NBSD-WSCS to examine the effect of seismic reinforcement. The results showed that the reference RC building with non-seismic details underwent shear collapse at seismic intensity of 200 cm/s^2. In the RC building with non-seismic details retrofitted with NBSD-WSCS, however, NBSD-WSCS with excellent energy dissipation capacity was able to accommodate about 42% of the total energy exerted on the test building. Thus, only minor seismic damage was expected. The major findings of the present study clearly indicated that this novel seismic retrofitting method using the NBSD-based WSCS has a high potential for commercialization.

Author Contributions: All authors have contributed to the development of the research and the elaboration of this article. Particularly, K.-S.L. contributed to the methodology and the experimental research, conceptualization, and edited the manuscript; B.-G.L. contributed to the experimental research and the dynamic analysis; J.-S.J. contributed to the methodology, the experimental research and the dynamic analysis. All authors have read and agreed to the published version of the manuscript.

Funding: This research received no external funding.

Institutional Review Board Statement: Not applicable.

Informed Consent Statement: Not applicable.

Data Availability Statement: All datasets generated in this study are available from the corresponding author upon reasonable request.

Acknowledgments: This paper was supported by a grant (2021R1A2C2094779) from the National Research Foundation of Korea, and a grant (2020-MOIS31-012) from the Fundamental Technology Development program for Extreme Disaster Response, funded by the Ministry of Interior and Safety of the Korean government.

Conflicts of Interest: The authors declare no competing interests.

References

1. Kobayashi, T.; Zen, K.; Yasufuku, N.; Nagase, H.; Chen, G.; Kasama, K.; Hirooka, A.; Wada, H.; Onoyama, Y.; Uchida, H. Damage to Residential RetainingWalls at the Genkai-Jima Island Induced by the 2005 Fukuoka-Ken Seiho-Oki Earthquake. *Soil Found.* **2006**, *46*, 793–804. [CrossRef]
2. Miyamoto, H.K.; Gilani, A.S.; Wada, A. Reconnaissance report of the 2008 Sichuan earthquake, damage survey of buildings and retrofit options. In Proceedings of the 14th World Conference on Earthquake Engineering, Beijing, China, 12–17 October 2008.
3. Sarrafzadeh, M.; Elwood, K.J.; Dhakal, R.P.; Ferner, H.; Pettinga, D.; Stannard, M.; Maeda, M.; Nakano, Y.; Mukai, T.; Koike, T. Performance of reinforced concrete buildings in the 2016 Kumamoto Earthquakes and seismic design in Japan. *Bull. N. Z. Soc. Earthq. Eng.* **2017**, *50*, 394–435.
4. Architectural Institute of Korea (AIK). Site Inspection and Damage Investigation of Buildings by Earthquakes in Gyoungju and Pohang, Seoul, Korea. *J. Korea Concr. Inst.* **2018**, *3*, 1–47.
5. *KDS 41*; Korean Design Standard. Architectural Institute of Korea: Seoul, Korea, 2019. (In Korean)
6. *FEMA 356*; Prestandard and Commentary for Seismic Rehabilitation of Buildings. FEMA: Washington, DC, USA, 2000.
7. Standard for Seismic Evaluation of Existing Reinforced Concrete Buildings, Guidelines for Seismic Retrofit of Existing Reinforced Concrete Buildings, and Technical Manual for Seismic Evaluation and Seismic Retrofit of Existing Reinforced Concrete Buildings. JBDPA: Tokyo, Japan, 2005.
8. SSRG (Seismic Strengthening Research Group). *Seismic Strengthening of RC Buildings*; SSRG, Ohmsha Press: Tokyo, Japan, 2008. (In Japanese)
9. Badoux, M.; Jirsa, O. Steel bracing of RC frames for seismic retrofitting. *J. Struct. Eng. ASCE* **1990**, *116*, 55–74. [CrossRef]

10. Nateghi-Alahi, F. Seismic strengthening of eight-storey RC apartment building using steel braces. *Eng. Struct.* **1995**, *17*, 455–461. [CrossRef]
11. Sugano, S. Seismic strengthening of existing reinforced concrete buildings in Japan. *Bull. N. Z. Soc. Earthq. Eng.* **1981**, *14*, 209–222. [CrossRef]
12. Ju, M.; Lee, K.S.; Sim, J.; Kwon, H. Non-compression cross-bracing system using carbon fiber anchors for seismic strengthening of RC structures. *Mag. Concr. Res.* **2014**, *66*, 159–174. [CrossRef]
13. Lee, K.S. An experimental study on non-compression X-bracing systems using carbon fiber cable for seismic strengthening of RC buildings. *Polymers* **2015**, *7*, 1716–1731. [CrossRef]
14. Smith, S.T.; Kim, S.J. Shear strength and behavior of FRP spike anchors in FRP-to-concrete joint assemblies. In Proceedings of the Fifth International Conference on Advanced Composite Materials in Bridges and Structures (ACMBS-V), Winnipeg, MB, Canada, 22–24 September 2008; ISBN 978-0-9736430-7-7.
15. Lee, K.S.; Lee, B.Y.; Seo, S.Y. A Seismic Strengthening Technique for Reinforced Concrete Columns Using Sprayed FRP. *Polymers* **2016**, *8*, 107. [CrossRef]
16. Lee, K.S. Experimental study on sprayed FRP system for strengthening reinforced concrete beams. *J. Adv. Concr. Technol.* **2012**, *10*, 219–230. [CrossRef]
17. American Society of Civil Engineers. *ASCE 7-10 (2010) Minimum Design Loads for Buildings and Other Structures*; ASCE (American Society of Civil Engineers): Reston, VI, USA, 2010.
18. Matsagar, V.A.; Jangid, R.S. Base Isolation for Seismic Retrofitting of Structures. *Pract. Period. Struct. Des. Constr.* **2008**, *13*, 175–185. [CrossRef]
19. Ferraioli, M.; Mandara, A. Base Isolation for Seismic Retrofitting of a Multiple Building Structure: Design, Construction, and Assessment. *Math. Probl. Eng.* **2017**, *2017*, 4645834. [CrossRef]
20. Bruno, S.; Valente, C. Comparative response analysis of conventional and innovative seismic protection strategies. *Earthq. Eng. Struct. Dyn.* **2002**, *31*, 1067–1092. [CrossRef]
21. Sahoo, D.R.; Rai, D.C. Seismic strengthening of non-ductile reinforced concrete frames using aluminum shear links as energy-dissipation devices. *Eng. Struct.* **2010**, *32*, 3548–3557. [CrossRef]
22. Ibrahim, Y.E.; Marshall, J.; Charney, F.A. A visco-plastic device for seismic protection of structures. *J. Constr. Steel Res.* **2007**, *63*, 1515–1528. [CrossRef]
23. Lee, C.-H.; Ryu, J.; Kim, D.-H.; Ju, Y.K. Improving seismic performance of non-ductile reinforced concrete frames through the combined behavior of friction and metallic dampers. *Eng. Struct.* **2018**, *172*, 304–320. [CrossRef]
24. Sutcu, F.; Takeuchi, T.; Matsui, R. Seismic retrofit design method for RC buildings using buckling-restrained braces and steel frames. *J. Constr. Steel Res.* **2014**, *101*, 304–313. [CrossRef]
25. Ramazan, O.; Yagmur, D.; Elif, E.F. The development of the buckling restrained braces with new end restrains. *J. Constr. Steel Res.* **2017**, *138*, 208–220.
26. Ferraioli, M.; Lavino, A. A Displacement-Based Design Method for Seismic Retrofit of RC Buildings Using Dissipative Braces. *Math. Probl. Eng.* **2018**, *2018*, 5364564. [CrossRef]
27. Eldin, M.N.; Dereje, A.J.; Kim, J. Seismic Retrofit of Framed Buildings Using Self-Centering PC Frames. *J. Struct. Eng.* **2020**, *146*, 04020208. [CrossRef]
28. Bedon, C.; Amadio, C. Passive Control Systems for the Blast Enhancement of Glazing Curtain Walls Under Explosive Loads. *Open Civ. Eng. J.* **2017**, *11*, 396–419. [CrossRef]
29. Bedon, C.; Amadio, C. Numerical assessment of vibration control systems for multi-hazard design and mitigation of glass curtain walls. *J. Build. Eng.* **2018**, *15*, 1–13. [CrossRef]
30. Bedon, C.; Amadio, C. ADAS dampers for the hazard protection of multi-storey buildings with glazing envelopes: A feasibility study. *Boll. Di Geofis. Teor. Ed. Appl.* **2019**, *60*, 197–220.
31. Ito, H.; Kasai, K. Passive control design for elasto-plastically damped building structure. In Proceedings of the Fifth International Conference on Behaviour of Steel Structures in Seismic Areas, STESSA 2006, Yokohama, Japan, 14–17 August 2006; Taylor & Francis Group: London, UK, 2006.
32. JSSI (Japan Society of Seismic Isolation). *JSSI Manual 2nd Edition: Design and Construction Manual for Passively Controlled Buildings*; Japan Society of Seismic Isolation: Tokyo, Japan, 2007.
33. Pu, W.; Kasai, K. Design Method for RC Building Structure Controlled by Elasto-Plastic Dampers Using Performance Curve. In Proceedings of the 15th World Conference on Earthquake Engineering, Lisbon, Portugal, 24–28 September 2012.
34. Kafi, M.A.; Hoosh, K.N. The geometric shape effect of steel slit dampers in their behavior. *Mag. Concr. Res.* **2019**, *3*, 3–17.
35. *KS B 0801*; Test Pieces for Tension Test for Metallic Materials. Korean Industrial Standards: Seoul, Korea, 2017. (In Korean)
36. *KS B 0802 (2018)*; Method of Tensile Test for Metallic Materials. Korean Standards Association: Seoul, Korea, 2018. (In Korean)
37. AIK (Architectural Institute of Korea). *Design Guideline and Examples of Seismic Energy Dissipating System*; AIK: Seoul, Korea, 2012. (In Korean)
38. Benavent Climent, A.; Oh, S.H.; Akiyama, H. Ultimate energy absorption capacity of slit-type steel plates subjected to shear deformations. *J. Struct. Constr. Eng.* **1998**, *503*, 139–145. [CrossRef]
39. Standard for Structural Calculation of Reinforced Concrete Structures. AIJ: Tokyo, Japan, 2010. (In Japanese)

40. Umemura, H. *Earthquake Resistant Design of Reinforced Concrete Buildings, Accounting for the Dynamic Effects of Earthquakes*; Giho-do Publishing Co.: Tokyo, Japan, 1973. (In Japanese)
41. Takanashi, K.; Udagawa, K.; Tanaka, H. Pseudo-dynamic tests on a 2-storey steel frame by a computer-load test apparatus hybrid system. In Proceedings of the 7th World Conference on Earthquake Engineering, Istanbul, Turkey, 8–13 September 1980.
42. Tokyo Soki Kenkyujo Company. Tokyo, Japan. 2020. Available online: https://www.tml.jp/e/ (accessed on 15 December 2021).
43. MTS Systems Corporation. *Pseudodynamic Testing for 793 Controllers*; MTS Systems Corporation: Eden Prairie, MI, USA, 2020.
44. Hilber, H.M.; Hughes, T.J.; Taylor, R.L. Improved numerical dissipation for time integration algorithms in structural dynamics. *Earthq. Eng. Struct Dyn.* **1977**, *5*, 283–292. [CrossRef]
45. Lee, K.S. Seismic capacity requirements for low-rise reinforced concrete buildings controlled by both shear and flexure. *J. Adv. Concr. Technol.* **2010**, *8*, 75–91. [CrossRef]
46. Lee, K.S.; Wi, J.D.; Kim, Y.I.; Lee, H.H. Seismic safety evaluation of Korean RC school buildings built in the 1980s. *J. Korean Inst. Struct. Maint. Insp.* **2009**, *13*, 149–159.
47. Standard for Damage Level Classification. JBDPA: Tokyo, Japan, 2017.
48. Maeda, M.; Nakano, Y.; Lee, K.S. Postearthquake damage evaluation for RC buildings based on residual seismic capacity. In Proceedings of the 13th World Conference on Earthquake Engineering, Vancouver, BC, Canada, 1–6 August 2004.
49. Jung, J.S.; Lee, K.S. A Seismic Capacity of RC Building Damaged by the 2016 Gyeongju Earthquake Based on the Non-linear Dynamic Analysis. *J. Korea Inst. Struct. Maint. Insp.* **2018**, *22*, 137–146.
50. Li, K.N. *Canny: A 3-Dimensional Nonlinear Dynamic Structural Analysis Computer Program, User Manual*; CANNY Structural Analysis Company: Vancouver, BC, Canada, 2009.
51. Matsumoto, Y.; Kitajima, K.; Nakanishi, M.; Adachi, H. A Study on Seismic Retrofit Design of Exiting RC Buildings by means of Friction Damper. *Trans. Jpn. Concr. Inst.* **2000**, *21*, 431–438.
52. Yokouchi, H.; Kitajima, K.; Nakanishi, M.; Adachi, H.; Aoyama, H. Experimental Study on Retrofit Effect of an Existing RC School Building Retrofitted with Energy Dissipation Devices. *J. Struct. Constr. Eng. (Trans. AIJ)* **2005**, *70*, 145–152. [CrossRef]
53. Jung, J.S.; Lee, K.S. A methodology for evaluating seismic capacity and seismic risk assessment of reinforced concrete buildings in Korea. *J. Asian Archit. Build. Eng.* **2020**, *19*, 103–122. [CrossRef]